International Journal of Biological Macromolecules 376 (2026) 153517

Contents lists available at ScienceDirect

International Journal of Biological Macromolecules

journal homepage: www.elsevier.com/locate/ijbiomac

Intranasal delivery of glioblastoma exosomes-loaded injectable chitosan hydrogel promotes neurovascular unit restoration in ischemic stroke

Lifei Huang [a], Zhihan Liu [a], Quanrui Zhang [a], Wensheng Xie [a], Guofeng Li [a], Junhao Yan [b], Meng Qin [a,c,**], Xing Wang [a,*]

[a] State Key Laboratory of Organic-Inorganic Composites, Beijing Laboratory of Biomedical Materials, Beijing University of Chemical Technology, Beijing, 100029, China
[b] Department of Human Anatomy, Histology and Embryology, School of Basic Medical Sciences, Peking University Health Science Center, Beijing, 100191, China
[c] Mental Health Center and Center for Preclinical Safety Evaluation of Drugs, West China Hospital, Sichuan University, Chengdu, 610041, China

ARTICLE INFO

Keywords:
Injectable chitosan hydrogel
Ischemic stroke
Neurovascular unit
Exosome
Intranasal delivery

ABSTRACT

The homeostasis of the Neurovascular Unit (NVU), a basic functional unit of the brain, is essential for neurological recovery. Glioblastoma-derived exosomes (Exos) have been demonstrated to enhance angiogenesis under hypoxic conditions, but their reparative potential in non-tumor ischemic microenvironments remain unclear. Moreover, free Exos are limited by rapid clearance, poor lesion retention, and uncontrolled release. Herein, we prepared an injectable chitosan hydrogel loaded with A172 cell-derived Exos (H-A-Exos) for intranasal delivery and evaluated its therapeutic effects in a rat middle cerebral artery occlusion (MCAO) model. *In vitro*, A-Exos facilitated endothelial cell proliferation, migration, and vascular endothelial growth factor (VEGF) expression, while inhibiting NVU cell apoptosis and reducing oxidative stress and inflammatory responses. When loaded within an injectable chitosan hydrogel, A-Exos exhibited enhanced retention and sustained release, resulting in improved accumulation in the ischemic infarct area following intranasal administration. Compared to the model group, H-A-Exos significantly improved behavioral recovery, as evidenced by a reduced modified Neurological Severity Score (mNSS), and decreased cerebral infarct volume (13.02 ± 1.01%), showing superior efficacy to free A-Exos and Nimodipine (NMDP). Mechanistically, H-A-Exos upregulated eNOS, Bcl-2, VEGF and CD31 expression, thereby promoting vascular regeneration and NVU remodeling. Thus, these findings confirm the effective pro-angiogenic and reparative roles of A-Exos in a non-tumor ischemic microenvironment and demonstrate that intranasal H-A-Exos represents a promising therapeutic strategy for restoring NVU homeostasis and enhancing revascularization following ischemic stroke, underscoring their innovative therapeutic potential.

1. Introduction

Ischemic stroke represents over 70% of all strokes globally [1], causing cell death and neurological deficit [2], with high rates of disability and significantly threatens human health [3–5]. During the acute phase of an ischemic stroke, the primary objective is to restore blood flow to the ischemic region to minimize damage [6–8]. Current treatments involve tissue plasminogen activator (tPA) and revascularization procedures [9–11]. However, these therapies have a narrow therapeutic window and can exacerbate neuronal cell death through oxidative stress and inflammation [10,12,13]. This phenomenon is known as ischemia/reperfusion (I/R) injury and can cause irreversible neuronal damage [14,15]. Actually, the brain is not a private ecological niche as traditionally thought. The Neurovascular Unit (NVU) is the basic functional unit of the brain, including neurons, glia (astrocytes, microglia), and vascular compartments (endothelial cells, pericytes), and represents a conceptual framework encompassing the neural and its adjacent vasculature system [16,17]. The NVU maintains brain homeostasis and cellular interactions in response to inflammation and disease by implementing coordinated vascular responses to central and peripheral signals [18]. Maintaining the function of cell types within the neurovascular unit (NVU) is essential for supporting NVU homeostasis

* Correspondence to: X. Wang, State Key Laboratory of Organic-Inorganic Composites, Beijing Laboratory of Biomedical Materials, Beijing University of Chemical Technology, Beijing 100029, China.
** Correspondence to: M. Qin, State Key Laboratory of Organic-Inorganic Composites, Beijing Laboratory of Biomedical Materials, Beijing University of Chemical Technology, Beijing 100029, China.
E-mail addresses: qinmeng212@scu.edu.cn (M. Qin), wangxing@mail.buct.edu.cn (X. Wang).

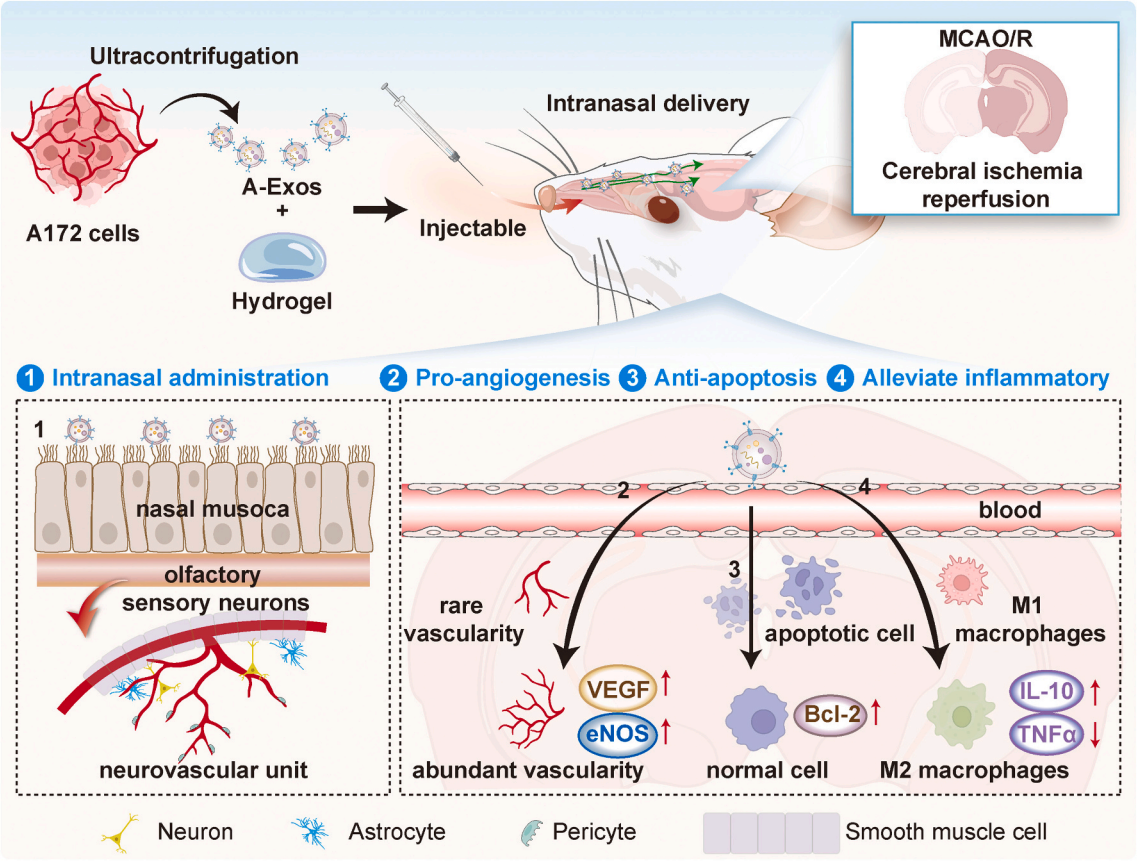
https://doi.org/10.1016/j.ijbiomac.2026.153517
Received 8 May 2026; Received in revised form 25 June 2026; Accepted 11 July 2026
Available online 13 July 2026
0141-8130/© 2026 Elsevier B.V. All rights are reserved, including those for text and data mining, AI training, and similar technologies.

[19], which facilitates neural regeneration and functional recovery after stroke, and represents a central focus of neuroprotective strategies [20,21]. Consequently, the development of safe and efficient therapeutic strategies to maintain NVU homeostasis has emerged as a pivotal focus of cerebral stroke repair.

Exosomes (Exos), nanoscale vesicles produced by cells, have emerged as an encouraging therapeutic strategy for brain diseases owing to their high biocompatibility, low immunogenicity, enhanced bioactivity, precise targeting and intercellular communication mediated [22–26]. Although Exos derived from mesenchymal stem cells [27,28] and other cells [29,30] have been widely investigated, tumor cell-derived Exos also exhibit strong pro-angiogenic effects by regulating endothelial cell proliferation, migration, and differentiation [31–33]. In particular, glioblastoma-derived Exos (GBM-Exos) contain angiogenic proteins that can be internalized by cerebrovascular endothelial cells and trigger robust angiogenic responses under hypoxic conditions [34–37]. Moreover, GBM-Exos can modulate macrophage polarization and inflammatory responses [38–40]. Reasonably, GBM-Exos may stimulate angiogenesis and promote NVU remodeling in ischemic stroke microenvironment. A172-derived exosomes have attracted increasing attention because of their ability to modulate angiogenesis and cellular remodeling [41], suggesting potential therapeutic value for neurovascular unit repair following ischemic stroke.

The intranasal pathway is a favorable strategy for delivering neuroprotective agents directly to the brain [42–44], particularly following reperfusion to mitigate ischemia-reperfusion (I/R) injury. By bypassing the blood-brain barrier (BBB) [45,46], intranasal administration can enhance bioavailability in the brain while avoiding gastrointestinal degradation and first-pass metabolism in the liver [47–52]. Recent studies have demonstrated that Exos can be effectively delivered to the infarcted area *via* intranasal administration [53,54], exerting neuroprotective effects on the ischemic brain [55–57]. For example, Zhou et al. improved the recovery of behavioral function after cerebral ischemia by intranasal delivery of BDNF-loaded small extracellular vesicles (sEVs), while stimulating angiogenesis and neural repair and reducing inflammation and infarct volume [57]. However, free Exos may still suffer from limited mucosal retention and rapid clearance from the nasal cavity. In this regard, Hydrogel-based delivery systems provide an effective strategy to overcome these limitations. Chitosan-based injectable hydrogels are particularly attractive owing to their biocompatibility, biodegradability, mild gelation, mucoadhesion, and sustained-release properties. As a three-dimensional Exos reservoir, injectable chitosan hydrogel can protect A-Exos from premature degradation, enable sustained release, and prolong nasal mucosal retention, thereby improving nose-to-brain delivery and enhancing therapeutic efficacy in ischemic brain injury.

Inspired by these, we prepared an injectable chitosan hydrogel loaded with A172 cell-derived Exos (H-A-Exos) for intranasal delivery and evaluated its therapeutic potential in a rat model of middle cerebral artery occlusion (MCAO) (Scheme 1). Given the tumor origin of A-Exos, this study also aimed to verify whether A-Exos could exert effective reparative functions in a non-tumor ischemic microenvironment. *In vitro*, A-Exos were investigated for their effects on endothelial cell proliferation, migration, VEGF expression, oxidative stress, inflammatory responses, and apoptosis under oxygen-glucose deprivation/reoxygenation (OGD/R) conditions, thereby assessing their pro-angiogenic and cytoprotective roles under non-tumor pathological conditions. The injectable chitosan hydrogel was designed to encapsulate A-Exos and achieve sustained release, thereby enhancing their retention and bioavailability. After intranasal administration, the brain distribution



Scheme 1. Schematic illustration of the therapeutic effects of intranasally delivered A172 cell-derived exosome-loaded injectable chitosan hydrogel (H-A-Exos) in ischemic stroke. Through intranasal administration, A-Exos released from H-A-Exos enhance endothelial proliferation and vascular remodeling, inhibit cell apoptosis, and reduce inflammation level, ultimately contributing to NVU restoration, neurological and functional recovery after cerebral ischemia.

and ischemic lesion accumulation of H-A-Exos were analyzed and compared with free A-Exos and Nimodipine (NMDP, a positive therapeutic agent in this study). Furthermore, the therapeutic efficacy of H-A-Exos was evaluated by behavioral assessment, infarct volume analysis, angiogenesis-related protein expression, vascular regeneration, and neurostructural repair. Hence, intranasal delivery of H-A-Exos could effectively promote angiogenesis, restore NVU homeostasis, and enhance neurovascular remodeling after ischemic stroke, supporting the therapeutic applicability of A-Exos in non-tumor environments and offering a promising alternative or adjunctive therapy for stroke recovery.

2. Methods

2.1. Chemicals and reagents

Inhaled isoflurane was purchased from Reward Life Science and Technology Co., Ltd., China. Glycol Chitosan ($\geq$ 80 kDa) was purchased from FUJIFILM Wako Chemicals Corporation). Aldehyde modified PEG was prepared according to the previous protocol [58]. Paraformaldehyde 4% (4% PFA), propidium Iodide (PI), 2′,7'-Dichlorofluorescin diacetate (DCFH-DA), 4′, 6diamidino-2-phenylindole solution (DAPI), Lacate Dehydrogenase (LDH) Activity Assay Kit, 2,3,5-triphenyltetrazolium chloride (TTC), annexin V-FITC/PI apoptosis detection kits were acquired from Solarbio Science & Technology Co.,Ltd., Beijing, China. Calcein AM was purchased from Biyuntian Biotechnology Co., Ltd., Shanghai, China. Nimodipine (purity 98%) was purchased from Yuanye Bio-Technology Co., Ltd., Shanghai, China. Penicillin sodium for injection was procured from Hengtong Dongbao Biotechnology Co., Ltd., Sichuan, China. BCA Protein Assay Kit, CCK-8 were purchased from Biorigin Inc., Beijing, China. Fetal bovine serum was acquired from Sigma-Aldrich Trading Co., Ltd., Shanghai, China. All media used for cell culture were purchased from Thermo Fisher Scientific Inc., Beijing, China.

2.2. Cell culture

Human glioblastoma cell lines (A172), Mouse Hippocampal Neuronal Cell Line (HT22), Human Neuroblastoma Cell Line (SH-SY5Y), and Human Umbilical Vein Endothelial Cells (HUVEC) were obtained from Servicebio Co., Ltd., Wuhan, China. Mouse C8-D1A Brain Astrocytes (C8-D1A) was obtained from Wuhan Pricella Biotechnology Co., Ltd. Brain-derived Endothelial cells.3 (bEnd.3) was purchased from National Collection of Authenticated Cell Cultures, China. Cells were removed from liquid nitrogen, thawed quickly in a water bath at 37 °C, resuspended with medium and inoculated in culture flasks, and cultured at 37 °C in a 5% CO_2 incubator. When the cell density reached 80%, the cells were passaged and inoculated in new culture flasks at appropriate ratios.

2.3. Purification and characterization of A-Exos

When the density of A172 cells reached 60%, the culture was changed to serum-free medium. After 48 h, A-Exos were obtained from the cell culture supernatant. Briefly, the supernatant was centrifuged at 300*g* for 10 min, 1200 g for 20 min, and 10,000 g for 30 min at 4 °C following by ultrafiltered for 30 min with an Amicon® Ultra filter (10 kDa MWCO) at 4000 g. Finally, the inner tube liquid was extracted by centrifugation using an ultrahigh-speed centrifuge (Beckman coulter, optima xpn-100 ultracentrifuge) at 100,000*g* for 2 h at 4 °C. The A-Exos pellet was re-suspended in D-PBS and analyzed by the BCA Protein Assay Kit to examine the protein concentration. For morphological analysis, A-Exos were examined by transmission electron microscope (TEM, Hitachi, HT7700) and scanning electron microscope (SEM, Tescan, MAIA3 XMU). A-Exos were tracked using Nanoparticle Tracking Analysis (NTA, Malvern Panalytical, NS500) and the Brownian motion of suspended A-Exos was measured, as well as the size distribution. Western blot (WB) analysis was used to detect A-Exos CD63 marker (Rabbit, PA5-100713, Thermo Fisher Scientific INC. USA), tumor susceptibility gene 101 (TSG 101, Rabbit, ab125011, Abcam, UK).

2.4. Preparation and characterization of CS hydrogel

Chitosan and Aldehyde modified PEG were dissolved separately in the exosome suspension, and then mixed to prepare a 1.75 wt% Schiff base-crosslinked CS hydrogel. The hydrogel was subsequently dispensed using a micropipette for injectability testing. The mechanical strength of the CS hydrogel was analyzed using a TA rotational rheometer. The storage modulus (G') and loss modulus of the hydrogel (G") were measured at 1% strain and 1 rad/s. Subsequently, step-strain analysis was performed on the CS hydrogel under alternating strain conditions of 1% strain and 600% strain to characterize its self-healing behavior. The microstructure of the H-A-Exos was examined using SEM. Release studies were performed using BSA model protein and A-Exos, respectively. BSA or A-Exos were incorporated into the CS hydrogel at a concentration of 5 mg/mL. The CS hydrogel was then immersed in 5 mL of PBS and incubated at 37 °C at 30 rpm. Samples were collected at predetermined time points, and the concentration was determined using a BCA Protein Assay Kit. The cumulative release amount was calculated based on the measured concentrations.

2.5. In vitro internalization assay

According to the manufacturer's guidelines, A-Exos were labelled using fluorescent dyes DiO, and then their uptake was examined through HUVEC, SH-SY5Y and HT22 cells. Cells were inoculated in confocal dishes at 1×10^5 cells/dish and incubated in a 5% CO_2 incubator at 37 °C for 24 h. Subsequently, DiO-labelled A-Exos were co-cultured with HUVEC, SH-SY5Y and HT22 cells. The incubation was ended at a fixed time point and the cells were fixed with paraformaldehyde, and re-stained with 100 μL of DAPI for nuclei, washed three times with PBS, and then observed by Confocal laser scanning microscope (CLSM, Leica, TCSSP8).

2.6. Cell proliferation evaluation

In order to detect the pro-proliferative effect of A-Exos, HUVEC cells in logarithmic growth phase were taken and inoculated in 96-well plates at a density of 8000 cells/well, and were cultured in a complete medium for 24 h. Subsequently, a gradient concentration of A-Exos was added, and the co-culture was continued for 22 h. After that, 10 μL of CCK-8 solution was applied to each well for 2 h. Absorbance at 450 nm was measured using the microplate readers (Tecan Trading AG, Switzerland).

2.7. Cell scratch assay

To detect the pro-cell migration effect of A-Exos, HUVEC cells were inoculated in 6-well plates at a density of 1×10^6 cells/well were incubated in a cell culture incubator for 24 h. Afterwards, a 10 μL pipette tip was used to make a scratch in the middle of the dish. Then the culture medium was replaced with a 2% FBS medium (with mitomycin added) for continued incubation. Addition of mitomycin A-Exos were added to the culture medium at this time and control group were left untreated. Subsequently, the scratch area was photographed at the specified time points using an inverted microscope after administration to analyze the cell migration efficiency.

2.8. Tube formation assay

Tube formation assay (TFA) is a classic method to study angiogenesis *in vitro*. Firstly, the matrix gel was thawed in the refrigerator at 4 degrees, and the gun head, centrifuge tube and well plate were pre-cooled

in advance. The 48-well plate was placed on an ice box, and 300 μL of pre-cooled matrix gel was added vertically into the plate, and the plate was gently shaken to distribute the gel evenly. After 1 h, HUVEC cells were added to each well at a concentration of approximately 1×10^6 cells/well, and then the plate was incubated at 37 °C. Afterwards, a light microscope was used to observe and take pictures at the specified time points. Based on the bright images, the relevant tube formation parameters (numbers master junction, total branches length and number meshes) were quantified by ImageJ software.

2.9. Oxygen-glucose deprivation/reoxygenation (OGD/R) model

The model of oxygen/glucose deprivation and reoxygenation (OGD/R) was established to simulate cerebral ischemia-reperfusion injury *in vitro* [59]. HT22 cells were inoculated in 96-well plates at a density of 1×10^4 cells/well, and cultured with DMEM complete medium (Wuhan Pricella Biotechnology Co., Ltd.) for 20 h to ensure complete apposition. To establish the OGD/R model, the cells were cultured in serum-free and glucose-free DMEM and then placed in an Anaerobic Jars (Mitsubishi Gas Chemical Company, INC, Japan) for 4 h, 6 h, 8 h. Subsequently, the cells were transferred to DMEM containing serum and glucose under normoxic conditions for 22 h. For the A-Exos group, cells were treated with A-Exos at a concentration of 400 μg/mL in 96 wells. The CCK-8 method was used for cell viability assessment. After perfused, 10 μL of CCK-8 solution was applied to each well, and the cells were incubated at 37 °C for 2 h. The absorbance was detected at 450 nm using the microplate readers.

Calcein AM/PI live/dead staining was applied to assess the survival of HT22 after OGD/R. The HT22 cells are inoculated into confocal culture dishes. Following OGD/R, cells were washed twice with PBS, and incubated with Calcein AM/PI staining solution in the dark for 20 min. Subsequently, CLSM was used for observation and photography. The OGD/R experiments for C8-D1A and bEnd.3 cells were performed according to the aforementioned protocol.

2.10. Reactive oxygen species (ROS) scavenging and anti-apoptosis ability

The neuroprotective activity of A-Exos was determined by measuring ROS scavenging and anti-apoptotic capacity. HT22 cells were inoculated in a black-bottomed, black-lidded 96-well plate and a confocal dish, followed by OGD/R-stressed. For the A-Exos group, cells were treated with A-Exos at a concentration of 400 μg/mL. After treatment, HT22 cells were stained with DCFH-DA for 20 min, and the cells were washed with fresh serum-free medium. Subsequently, cells were visualized using an inverted CLSM. The fluorescence intensity was read at excitation 488 nm and emission 525 nm in a multi-mode microplate detection system (Perkin elmer, USA).

The cell apoptosis was then measured by using the Annexin V-FITC/PI apoptosis detection kit according to the manufacturer's instructions. The OGD/R-stressed HT22 cells were washed and then centrifuged at 1000 rpm for 5 min. Then, the cell precipitates were resuspended and incubated continuously with Annexin V-FITC and PI for 15 min at room temperature in the dark. The early and late apoptotic cells was detected using the flow cytometer (ID7000Spectral cell analyzer, SONY, Japan).

2.11. L-lactate dehydrogenase (L-LDH) activity assay

The concentration of L-LDH was determined using the L-LDH activity assay kit. Pyruvate standards were diluted to gradient concentrations (2, 1, 0.5, 0.25, 0.125, 0 μmol/mL) and subsequently cultures of each group of cells were collected and assayed according to the kit and L-LDH activity was calculated according to the number of cells.

2.12. ELISA assay for inflammatory cytokines assessment

RAW264.7 cells were induced to polarize toward M1-type with LPS (1 μg/mL) for 12 h and recover for 6 h. A-Exos were utilized to protect RAW264.7 cells from M1. Then the conditional medium of RAW 264.7 cells was centrifuged to remove cells and subjected to TNFα, IL-1β, IL-6, IL 10 ELISA Kits (Invitrogen, Thermo Fisher Scientific INC. USA). Readings from each sample were normalized to the protein concentration.

2.13. Preparation of rat MCAO/R model

Healthy male Sprague-Dawley rats weighing 280–330 g were selected and purchased from Viton Lihua Laboratory Animal Technology Co., Ltd., Beijing, China. The animals were kept at a temperature of (22 ± 3)°C, fasted for 12 h before the operation, and drank water freely. All animal experiments were conducted by the National Research Council's Guide for the Care and Use of Laboratory Animals ethically and approved by the Peking University Institutional Animal Care and Use Committee (LA2019083).

The rat MCAO model was prepared by the wire embolism method, and the common carotid artery-inner carotid artery-middle cerebral artery pathway was used for modelling. The surgical procedure was as follows: The animals were anesthetized with inhalation of isoflurane (RWD, Shenzhen, CN). Following the gentle separation of the carotid arteries, a suture was tied at the proximal end of the main trunk of the common carotid artery and the nylon bolus wire (XINONG Technology Co., Ltd., Beijing, China.) was inserted slowly along the common carotid artery. Then the suture was sent along the internal carotid artery to the middle cerebral artery and stop inserting until there is slight resistance. Sutures were removed after 90 min to allow reperfusion. Following the operation, penicillin sodium was applied to prevent infection. Besides the suture insertion and occlusion, sham group rat underwent the same surgery.

Neurological scoring of rat was performed according to the Longa 5-point scale [60]. 0 points: no symptoms of neurological damage; 1 point: the contralateral forepaw could not be fully extended; 2 points: circling to the contralateral side; 3 points: leaning to the contralateral side, walking with difficulty; 4 points: inability to walk spontaneously, loss of consciousness; 5 points: death. Inclusion criteria: 1. Score: 1–3 points; 2. No subarachnoid hemorrhage. Those who did not meet the criteria were excluded.

2.14. Intranasal drug administration and behavioral evaluation

The experimental animals were randomly divided into 5 groups: the sham operation group, the MCAO group, the NMDP group, the A-Exos group and the H-A-Exos group. The first treatment was administered immediately after reperfusion. The subsequent two treatments were performed 24 and 48 h after surgery. During each treatment, 20 μL of H-A-Exos and free A-Exos at a concentration of 1×10^{10} particles/mL were delivered intranasally to the nostrils of rat. The NMDP was administered at a concentration of 4 mg/kg. For rat in the MCAO group, they received 20 μL of PBS in the same way, and the sham group received no treatment.

Motor function, sensory function, and reflexes were assessed daily for the next 7 days using the modified Neurological Severity Score (mNSS) [61]. The total score of the scale was 0–18, and the severity was graded as follows: 13–18 indicated severe impairment; 7–12 indicated moderate impairment; and 1–6 indicated mild impairment.

7 days after MCAO treatment, the 2% Evans blue solution (4 mL/kg) was injected into the tail vein of each group of rats. After injection, the solution circulated in the rats' bodies for 3 h, followed by cardiac perfusion with 0.9% sodium chloride solution (containing heparin). The brain tissue was collected to observe Evans blue leakage. The tissue was further homogenized, and the supernatant was measured for absorbance

at 620 nm. Other brain tissues were snap-frozen at −20 °C for 20 min, and the brain was subsequently coronal sectioned into five 2 mm slices using a tissue sectioning knife. Infarct volume was subsequently assessed by 2,3,5-triphenyltetrazolium chloride (TTC) staining for 10 min. The percentage of infarct was calculated by the formula (1). The infarct volume was calculated for each group of rats and expressed as a percentage of the total section volume.

$$\text{Infarct volume ratio} = \frac{\text{sum of sectioned infarct volume}}{\text{sum of sectioned brain volume}} \times 100\% \quad (1)$$

Inflammatory factors (TNFα, IL10) of brain tissue were determined by ELISA (IL 10, Invitrogen, Thermo Fisher Scientific INC. USA; TNFα, Servivebio Co., Ltd., Wuhan, China). The eNOS, BCL-2, CD31, Vascular endothelial growth factor (VEGF) protein content of brain tissue was measured by WB. Equal amounts of proteins were loaded and separated with sodium dodecyl sulfate-polyacrylamide gel electrophoresis (SDS-PAGE) and then transferred to polyvinylidene fluoride membranes (Millipore, Germany) by electrophoresis apparatus (JY300HE, Beijing Junyi Electrophoresis Co., Ltd). Primary antibodies (Servicebio Co., Ltd., Wuhan, China) used in this study were rabbit polyclonal anti-CD31, rabbit polyclonal anti-VEGF, and rabbit polyclonal anti-β-actin. The membranes were incubated with peroxidase-conjugated secondary antibodies (HRP conjugated Goat Anti-Rabbit IgG (Servicebio Co., Ltd., Wuhan, China)), and the bound proteins were visualized using enhanced chemiluminescence (Tanon 5200).

2.15. In vivo tracing study

To observe the targeting effect and prolonged retention, H- A-Exos and A-Exos stained with Cy7.5 was administered *via* intranasal drops, and an equal volume of PBS was injected into the control group. The fluorescence intensity of the head was observed by *in vivo* fluorescence imaging at 0, 1, 2, 4, 6, 12 h post-injection. After 2 h, 6 h observation, the rats were dissected and the brain, heart, liver, spleen, lungs, and kidneys were exposed by IVIS Spectrum (Caliper life sciences. USA) to obtain fluorescence images. The fluorescence intensity at different time points was then analyzed using Living Image software. To improve the immunostaining results of the sections, H-A-Exos and A-Exos was stained with CY7-SE, and brain tissue sections were harvested at 2 and 6 h for immunostaining.

2.16. Histopathological examination and immunofluorescence staining

After anesthesia, the brains of rats were isolated after cardiac perfusion with 0.9% saline and 4% PFA. The brains were embedded in paraffin and snap-frozen at −20 °C after sucrose dehydration, and then coronal cut into 2 μm thick sections. Brain sections were washed 3 times with PBST and incubated with CD31 antibody, VEGF antibody, Iba1 antibody or NeuN antibody (Servicebio Co., Ltd., Wuhan, China) at 4 °C overnight. After washing 3 times with PBST, these brain sections were incubated with different secondary antibodies for 1 h at room temperature. Then the sections were then blocked with blocking medium containing DAPI and imaged by CLSM. The histopathology of brains histopathology by H&E and Nissl staining to detect morphological features of tissues and damaged neurons. Brain sections (2 μm) were stained with H&E and Nissl reagent, and images were observed under biomicroscope. In addition, TUNEL staining was performed to assess apoptosis in brain regions using the TUNEL Apoptosis Detection Kit (Servicebio Co., Ltd., Wuhan, China).

2.17. Statistical analysis

All the data in this work were presented as the mean ± standard deviation (SD). Comparisons of means between two groups were analyzed by unpaired Student's *t*-test while among multiple groups by one-way analysis of variance (ANOVA). Two-tailed p value <0.05 was considered statistically significant.

3. Results and discussion

3.1. Preparation and characterization of A-Exos and H-A-Exos

The successful isolation and characterization of Exos are crucial for subsequent investigations into their therapeutic potential. The A-Exos were isolated from the conditioned medium of A172 cells culture by using typical density gradient centrifugation and ultracentrifugation (Fig. 1a). The A-Exos exhibited a characteristic cup-shaped morphology under SEM and TEM observation (Fig. 1b, 1c), with diameters ranging from 100 to 200 nm. NTA confirmed that the size distribution of the A-Exos solution fell within the range of 50 to 200 nm (Fig. 1d). WB analysis further validated the successful isolation of A-Exos, revealing enrichment of the markers CD63 and TSG101, which are established indicators of A-Exos biogenesis (Fig. 1e). These findings prove that A-Exos exhibit the typical morphology, size, and protein marker expression.

To enhance the retention and sustained release of A-Exos, an injectable CS hydrogel loaded with A-Exos (H-A-Exos) was prepared. As shown in Fig. 1f, the hydrogel network was constructed through a dynamic Schiff-base reaction between the amino groups of glycol chitosan and the aldehyde groups of aldehyde-functionalized PEG The formation of reversible imine bonds (-CH=N-) was confirmed by NMR spectroscopy (Fig. S1). During gelation, A-Exos were physically encapsulated within the three-dimensional hydrogel network. An inverted vial test demonstrated that the precursor solution forms a stable hydrogel upon mixing (Fig. 1g). Furthermore, the CS hydrogel can be smoothly extruded through a syringe and retains its shape after injection, confirming its excellent injectability (Fig. 1g). The microstructure of the hydrogel was further examined *via* SEM. The lyophilized hydrogel exhibited an interconnected porous structure with abundant micropores (Fig. 1h). This porous structure facilitates water absorption, nutrient diffusion, and the loading of exosomes. At higher magnifications, numerous nanoscale spherical particles were observed on the hydrogel scaffold, indicating that A-Exos were successfully incorporated and retained within the hydrogel matrix (Fig. 1i). Rheological analysis showed that the storage modulus of H-A-Exos was approximately 200 Pa, indicating suitable mechanical compliance with mucosal tissues (Fig. 1j). Step-strain rheological testing further revealed a reversible sol-gel transition, suggesting excellent self-healing behavior (Fig. 1k). This property allows H-A-Exos to flow under shear stress during injection and rapidly recover its gel structure afterward, which is beneficial for local retention and sustained delivery. BSA and A-Exos were used to evaluate the release behavior of bioactive payloads from hydrogels. As shown in Fig. 1l and Fig. S2, both BSA and A-Exos exhibited typical biphasic release curves, characterized by an initial burst release followed by a sustained-release phase. The overall release trends were highly consistent; in both cases, >80% of the loaded cargo was released within 24 h. The cumulative release gradually increased and approached near-complete release at later time points. This sustained-release behavior may reduce the rapid clearance of A-Exos and prolong their retention on the nasal mucosa, thereby improving their potential for intranasal delivery.

3.2. The effect of A-Exos on HUVEC migration and tube formation

Angiogenesis plays a crucial role in the treatment of cerebral ischemia. We utilized DiO-labelled A-Exos to assess their time-dependent uptake in HUVEC cells at various time points. As shown in Fig. 2a, HUVECs progressively internalized A-Exos in a time-dependent manner. Moreover, SH-SY5Y cells and HT22 cells, representing typical nerve cell models, also internalized A-Exos (Fig. S3, S4). Interestingly, A-Exos promoted cell proliferation, but not in a dose-dependent manner (Fig. S5). The scratch wound assay was performed to assess the bioactivity of A-Exos on HUVEC migration. The results supported that A-Exos

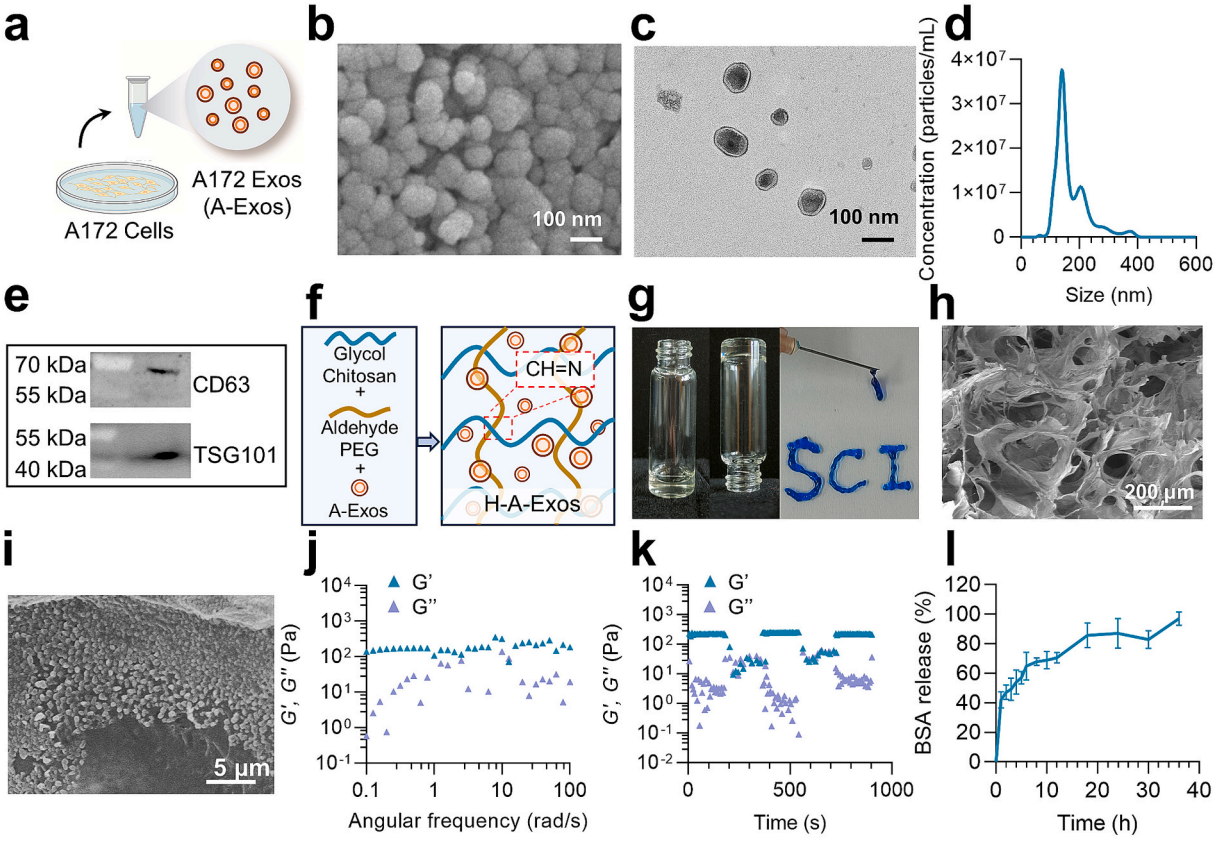


Fig. 1. Preparation and characterization of A-Exos and H-A-Exos. (a) Schematic illustrates the preparation of A-Exos. (b) Morphology of A-Exos under SEM and (c) TEM. Scale bar: 100 nm. (d) Representative results of the average particle concentration and size distribution following NTA. (e) WB show protein expression in A-Exos, including specific markers (CD63 and TSG101). (f) Schematic illustration of the preparation of injectable chitosan hydrogel loaded with A-Exos (H-A-Exos). (g) Photographs showing hydrogel formation by the inverted vial test and injectability of H-A-Exos through a syringe. (h) SEM image of the lyophilized hydrogel and (i) nanoscale A-Exos retained on the hydrogel. (j) Frequency sweep rheological analysis and (k) step-strain rheological analysis of H-A-Exos. (l) *In vitro* release profile of BSA from the hydrogel.

significantly enhanced HUVEC migration, as evidenced by a reduction in wound area compared to the control group (Fig. 2b, c). Notably, the healing rate in the A-Exos group approached 100% after 48 h, representing an approximate 1.5-fold increase over the control. To evaluate the pro-angiogenic capacity of A-Exos, a tube formation experiment was conducted. The HUEVC-formed tube images were adopted by an inverted microscope (Fig. 2d). The software analysis revealed that A-Exos significantly increased the number of junctions, total branch length, and mesh formation compared to the control group (Fig. 2e, f, Fig. S6). Due to these visible results, A-Exos have a pronounced effect on facilitating angiogenesis.

3.3. *Anti-apoptosis assessment in OGD/R-stressed NVU cells*

Subsequent experiments focused on the therapeutic effect of A-Exos on hypoxic injury. Cell viability and cytotoxicity were analyzed using Calcein AM/PI live/dead staining and CCK-8 assay. To investigate whether A-Exos are involved in neuroprotection, HT22 cells were subjected to OGD for 1 h, 4 h, 6 h, and 8 h, followed by a 21 h re-oxygenation period. Light microscopy visualized the loss of HT22 cell morphology and an increase in apoptotic cells after OGD/R (Fig. S7). The cell viability decreased with prolonged OGD/R duration (Fig. 3a). To identify the optimal A-Exos concentration for cell recovery, we evaluated their effects under the most severe OGD/R condition (8 h). While lower concentrations of A-Exos did not yield significant differences in cell viability, increasing the concentration to 200 μg/mL led to notable improvements (Fig. 3b). At concentrations of 400 μg/mL and 800 μg/mL, cell viability was significantly higher than at 200 μg/mL, though no distinct difference was observed between the two higher concentrations. Thus, 400 μg/mL was selected for subsequent experiments. The non-dose-dependent proliferative effect may be attributed to receptor saturation and limitations in cellular uptake, suggesting that even moderate concentrations of A-Exos are sufficient to induce maximal biological responses. The CCK-8 results showed that A-Exos treatment improved cell survival rates compared to the OGD/R group by 23.94 ± 4.28% (1 h), 22.02 ± 1.59% (4 h), 27.39 ± 0.93% (6 h), and 23.50 ± 7.86% (8 h) (Fig. 3c, Fig. S8). To establish a moderate-to-severe injury model for clearly observing the neuroprotective rescue effects of A-Exos, an OGD/R duration (4 h, 43.03%) corresponding to approximately 50% cell viability was selected [62]. Under these conditions, the effects of A-Exos on astrocytes (C8-D1A cells) and microvascular endothelial cells (bEnd.3 cells) were further investigated. Fig. 3c showed that under OGD/R-stressed, A-Exos increased the viability of C8-D1A cells by 17.77 ± 3.67% and that of bEnd.3 cells by 14.58 ± 6.69%. Additionally, A-Exos significantly reduced neuronal cells, astrocytes and microvascular endothelial cells apoptosis and enhanced their viability through Calcein AM/PI staining (Fig. 3d, Fig. S9). Flow cytometric assay further demonstrated a 5.6 ± 1.18% reduction in apoptosis following A-Exos treatment (Fig. 3e, f). This revealed the reduction of NVU cell viability and cytotoxicity under OGD/R-stressed could be reversed by applying A-Exos. A-Exos are highly efficient to mitigate hypoxic injury by promoting NVU cell viability and reducing apoptosis, prompting further investigation into their underlying mechanisms.

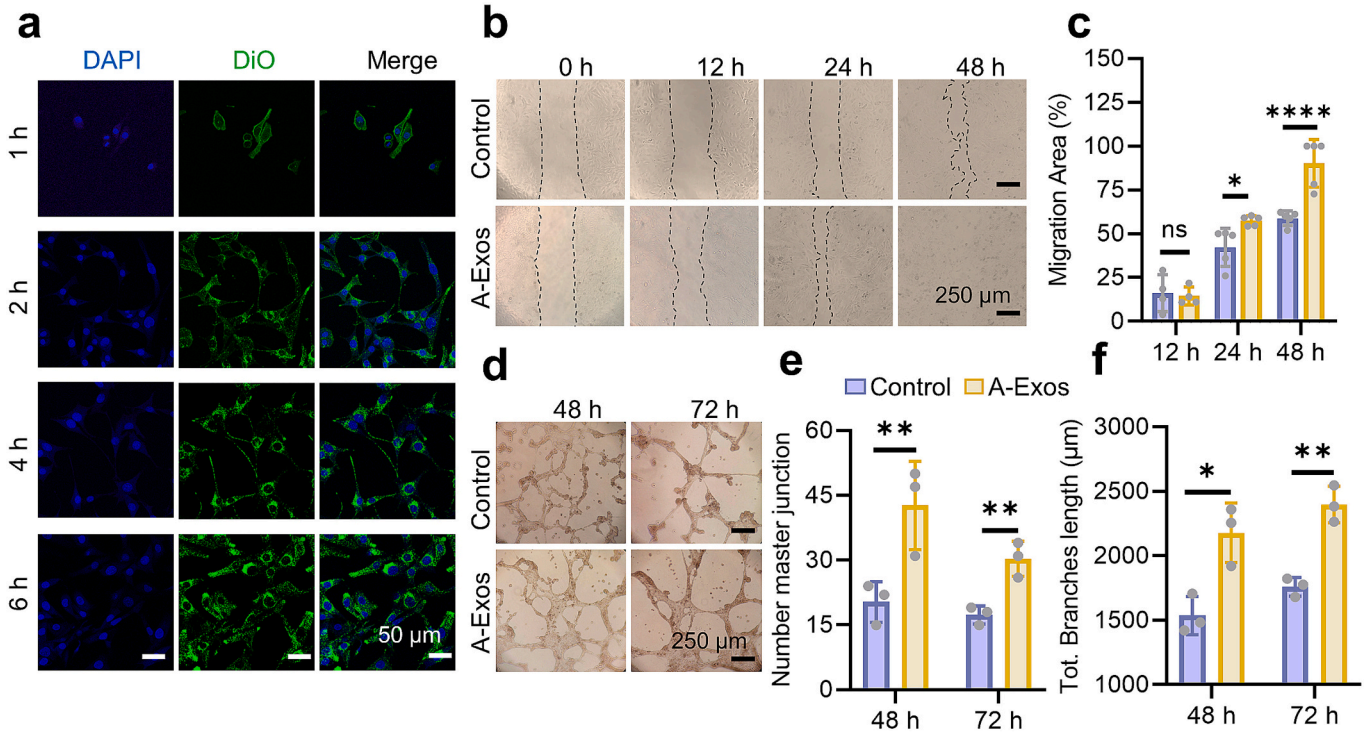


Fig. 2. The internalization, migration promotion, and tube-forming capacity of A-Exos. (a) Fluorescence microscopy analysis of DiO-labelled A-Exos internalization in HUVECs. (Green: DiO, blue: DAPI). (b) The effects of A-Exos on the migration of HUVECs. (c) Scratch healing area analysis ($n = 4$–5). (d) The light microscopy of tube formation of HUVECs in matrix gels that assess the pro-angiogenic properties of A-Exos. (e) Statistical analyses of master junction ($n = 3$) and (f) total branches length (n = 3). Data are expressed as the mean ± SD, ****$p < 0.0001$, **$p < 0.01$, *$p < 0.05$. ns: $p > 0.05$.

3.4. ROS elimination and anti-inflammatory assessment

Following cerebral ischemia, ROS rapidly increases and overwhelms antioxidant defenses, eventually leading to neuronal apoptosis and necrosis. Oxidative stress activates inflammatory signaling pathways, exacerbating blood-brain barrier disruption and secondary damage. Given these detrimental effects, combating oxidative stress is essential in the treatment of cerebral ischemia. Therefore, the antioxidative capacity of A-Exos were evaluated in this pathological context. DCFH-DA staining was employed to measure intracellular ROS levels. OGD/R treatment group greatly increased the ROS release in cells with enhanced fluorescence (Fig. 4a). The A-Exos treatment group reduced the ROS level with comparably fluorescence level to the control group (without special treatment). The quantitative results obtained a 59.90% ± 5.68% reduction in ROS levels after A-Exos treatment in comparison to OGD/R (Fig. 4b). As such, A-Exos may be effective in maintaining redox homeostasis under ischemic conditions.

Beyond their antioxidative function, A-Exos were also investigated for their ability to reduce neuronal damage. Lactate dehydrogenase (L-LDH) release, a well-established marker of cell injury, was quantified to evaluate cellular protection [63]. As shown in Fig. 4c, among the three cell types composed of the NVU, A-Exos treatment led to a decrease in cell death compared to the control group. Since oxidative stress and inflammation are closely interconnected, we also examined the anti-inflammatory effects of A-Exos in RAW264.7 cells. These macrophages were polarized to an M1 pro-inflammatory phenotype using LPS stimulation. Notably, treatment with A-Exos after LPS exposure resulted in notably reduced production of pro-inflammatory cytokines, including TNF-α, IL-1β, and IL-6 (Fig. 4d-f). Furthermore, the anti-inflammatory efficacy of A-Exos was greater than that of the untreated group (Fig. 4 g). Consequently, the multifaceted protective effects of A-Exos as they protect neurons from hypoxic damage by enhancing cell viability and reducing apoptosis. These results provide a basis for further investigation into the therapeutic potential of A-Exos in cerebral ischemia.

3.5. Intranasally-delivered H-A-Exos target to the ischemic brain

For assessing the *in vivo* targeting capability of A-Exos to the ischemic brain, MCAO/R was performed in the right hemisphere of the brain of SD rats. As shown in Fig. 5a, the green fluorescence of DiO labelling and the red fluorescence of Cy7.5 labelling almost overlap, which suggests that A-Exos can be labelled by dual dyes. To further track the biodistribution of A-Exos, Cy7.5-labelled A-Exos were first visualized using an IVIS system, which detected strong fluorescence signals, confirming that A-Exos were effectively labelled and suitable for subsequent *in vivo* tracking (Fig. 5b). The intranasal retention behavior of free A-Exos and H-A-Exos was then investigated by *in vivo* fluorescence imaging at different time points after administration. As shown in Fig. 5c, free A-Exos rapidly appeared in the nasal region at 1 h, but the fluorescence intensity gradually decreased over time, indicating relatively fast clearance from the nasal cavity. In contrast, H-A-Exos exhibited stronger and more persistent fluorescence signals in the nasal region from 1 to 6 h. Quantitative analysis further confirmed that, in the early and middle phases following administration, the average fluorescence intensity of H-A-Exos was higher than that of free A-Exos (Fig. 5d). This indicates that the injectable chitosan hydrogel significantly enhanced the retention of A-Exos in the nasal mucosa and delayed their clearance. To further evaluate systemic distribution, major organs were collected 2 and 6 h after intranasal administration and analyzed using fluorescence imaging. As shown in Fig. 5e, free A-Exos were primarily detected in the brain and metabolic organs, including the liver and kidneys, suggesting that brain delivery was accompanied by systemic distribution and clearance. In contrast, H-A-Exos exhibited stronger fluorescence signals in the brain at 2 and 6 h, indicating improved brain accumulation. Fluorescence signals were also observed in the liver and kidneys (Fig. S10). The total radiant efficiency of the liver is the highest, which is closely related to the size of the organ. It should be noted that a portion of A-Exos undergo systemic clearance primarily through renal and hepatic pathways, a common fate for nanoparticles and exosome. The

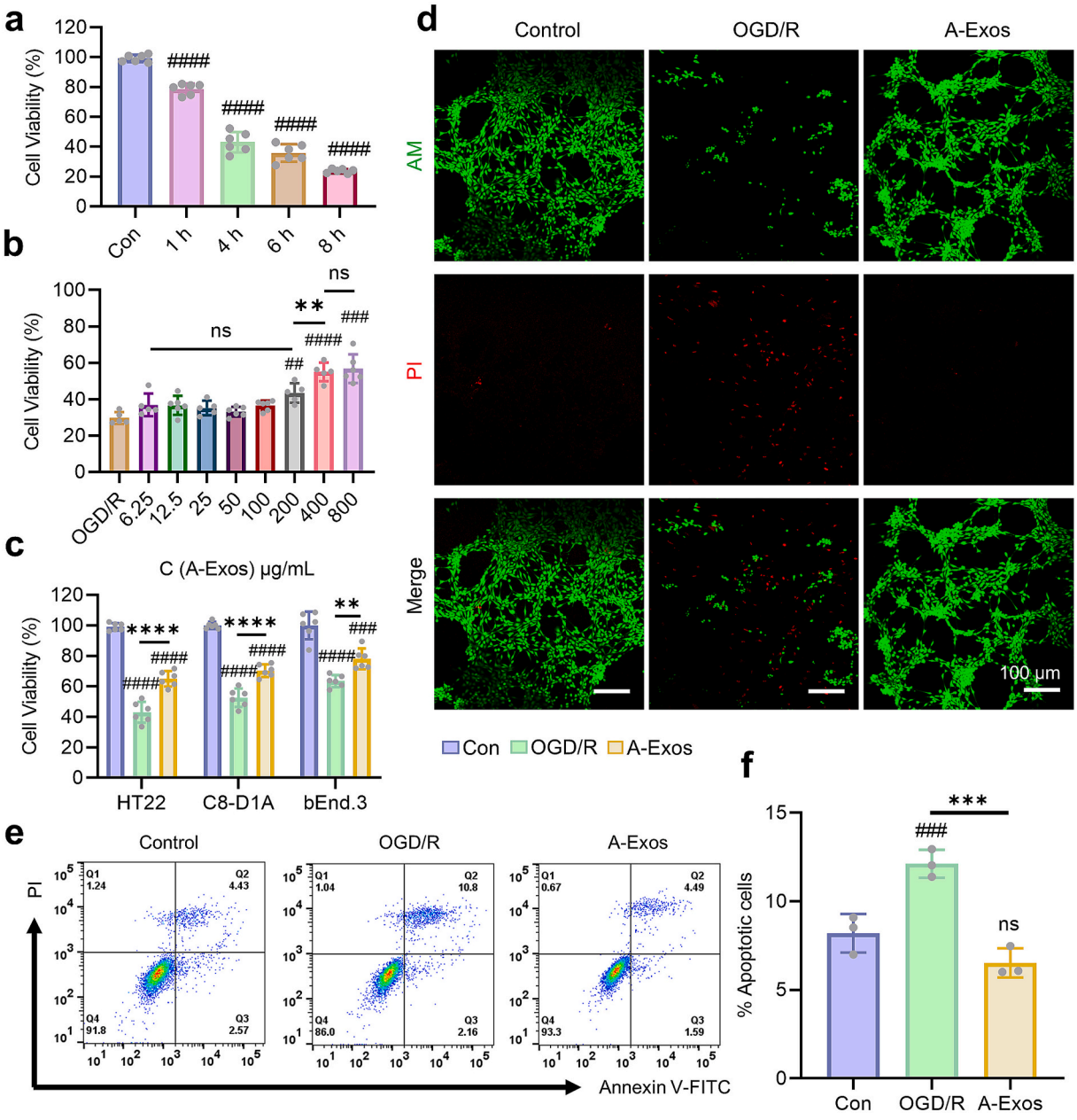


Fig. 3. The A-Exos inhibits apoptosis and improves cell viability. (a) Cell viability at different OGD/R test times ($n = 6$). (b) Cell viability upon A-Exos treatment with graded concentrations following 8 h of OGD/R-stressed ($n = 5$–6). (c) Cell viability of A-Exos treated HT22 cells, C8-D1A cells and bEnd.3 cells after 4 h of OGD/R-stressed (n = 6). (d) The live/dead staining of HT22 cells in control, OGD/R and A-Exos treated groups. (e) Annexin V/PI double staining followed by flow cytometry analysis of HT22 cell apoptosis in response to A-Exos or PBS treatment under OGD/R stress and (f) the quantification of apoptosis cells ($n = 3$). Data are expressed as the mean ± SD, # means the contrasts between experimental groups and control. $^{\#\#\#\#/****}p < 0.0001$, $^{\#\#\#/***}p < 0.001$, $^{\#\#/**}p < 0.01$, ns: $p > 0.05$.

higher brain fluorescence intensity in the H-A-Exos group supports the role of CS hydrogels in enhancing nasal-to-brain delivery efficiency by prolonging nasal retention time and sustaining the release of A-Exos.

The distribution of A-Exos within brain tissue and their interactions with NVU-associated cells were further investigated by immunofluorescence staining. In A-Exos and H-A-Exos group, the fluorescence signal showed strong colocalization with multiple brain cell-specific markers, including CD34-positive endothelial cells, GFAP-positive astrocytes, Iba1-positive microglia, and NeuN-positive neurons (Fig. 5f). These results indicate that intranasally delivered A-Exos can penetrate brain tissue and be effectively internalized by major NVU-associated cell types. Endothelial uptake may enable A-Exos to regulate vascular function and blood-brain barrier integrity, while their colocalization with astrocytes and microglia suggests potential involvement in modulating glial activation and neuroinflammation. In addition, neuronal uptake provides cellular evidence for the direct neuroprotective effects of A-Exos. Consistent with the IVIS imaging results, these immunofluorescence findings further confirm that A-Exos reach ischemic brain regions, enter the brain parenchyma, and interact with multiple NVU components rather than merely remaining within the vascular lumen or undergoing nonspecific retention. Finally, H&E staining was performed on nasal mucosal tissues collected from rats treated with PBS (negative control), NMDP, A-Exos and H-A-Exos respectively, for evaluating the safety of intranasal A-Exos administration (Fig. S11). The PBS group displayed an intact nasal mucosal structure with well-organized cells. Similarly, the A-Exos and H-A-Exos group exhibited no noticeable abnormalities in mucosal architecture, implying that intranasal delivery of A-Exos did not induce detectable

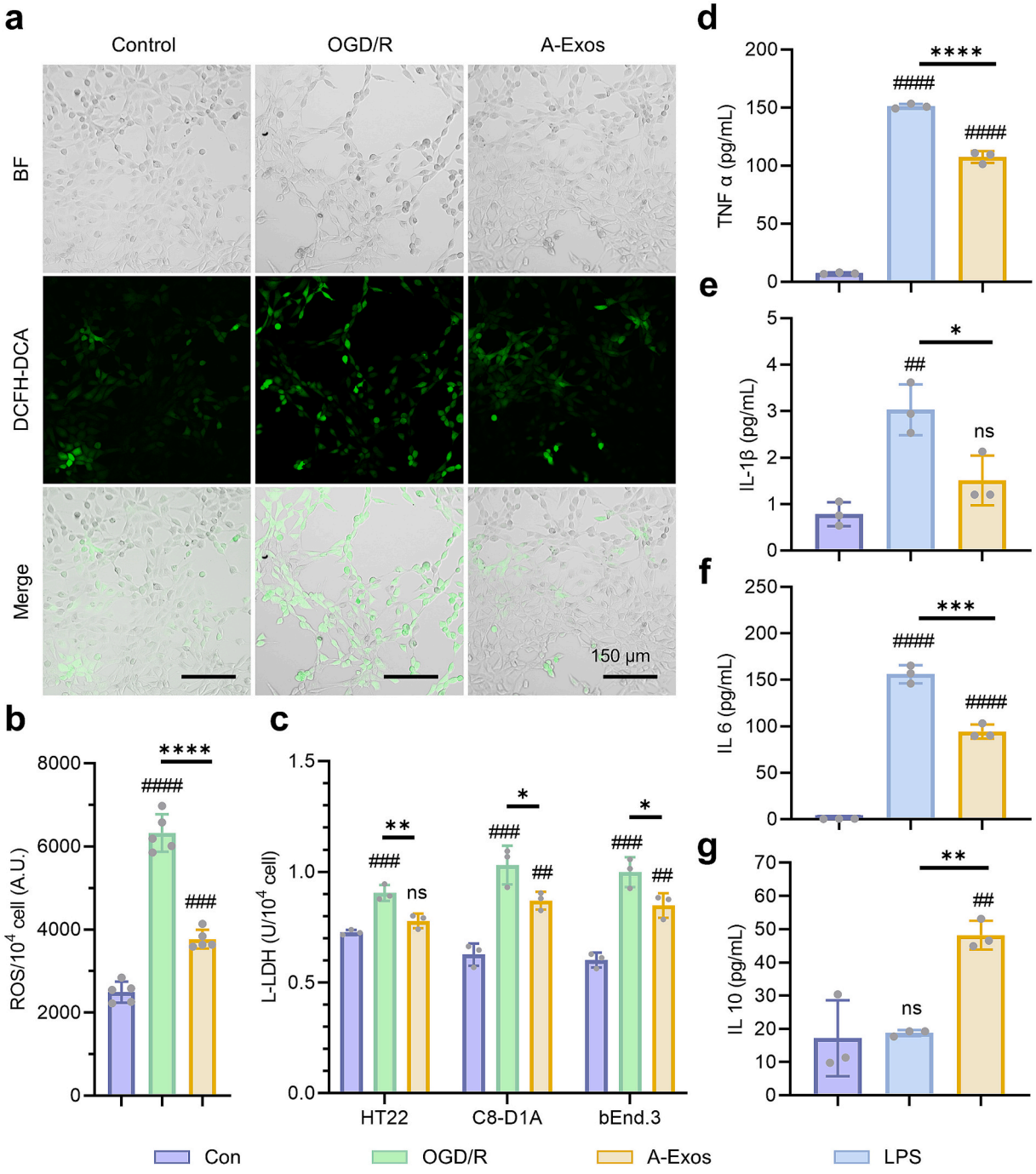


Fig. 4. The effects of A-Exos for ROS elimination and anti-inflammatory. (a) Evaluation of intracellular ROS generation by DCFH-DA staining and (b) the quantification of ROS generation by multi-mode microplate detection system ($n = 5$). (c) The LDH release of HT22 cells, C8-D1A cells and bEnd.3 cells under OGD/R stress ($n = 3$). ELISA analyses (n = 3) of (d) TNF α, (e) IL-1β, (f) IL 6 and (g) IL 10 in the conditioned medium were performed after LPS-induction. Data are expressed as the mean ± SD, # means the contrasts between experimental groups and control. $^{\#\#\#\#/****}p < 0.0001$, $^{\#\#\#/***}p < 0.001$, $^{\#\#/**}p < 0.01$, $^{\#/*}p < 0.05$, ns: $p > 0.05$.

toxicity or structural damage to the nasal mucosa.

3.6. H-A-Exos reduces infarct volume and improves behavioral recovery post-MCAO

The effect of A-Exos on ischemic strok ischemic stroke rats e rats *in vivo* was further investigated. An experimental schedule was designed as illustrated in Fig. 6a, with the MCAO/R model establishment detailed in Fig. S12. NMDP, a recognized therapeutic agent for ischemic stroke, served as a *in vivo* positive control [64,65]. The ischemic brain regions appeared pale post-MCAO/R, clearly distinguishing them from normal tissue (Fig. 6b), which confirming successful model establishment. The integrity of cerebral microvasculature was further assessed by Evans blue staining. Evans blue assay showed significant dye leakage in the MCAO group, which was substantially reduced by both NMDP, A-Exos and H-A-Exos treatments (Fig. S13a). Quantitative analysis of Evans blue leakage at 620 nm showed that the absorbance in the MCAO/R group increased to 0.366 ± 0.060 (Fig. S13b), significantly higher than that in the sham group 0.166 ± 0.017. In contrast, absorbance values decreased in the NMDP, A-Exos, and H-A-Exos groups to 0.246 ± 0.050, 0.249 ± 0.027, and 0.196 ± 0.011, respectively. Among them, H-A-Exos was closest to the normal level, suggesting its superior ability to preserve

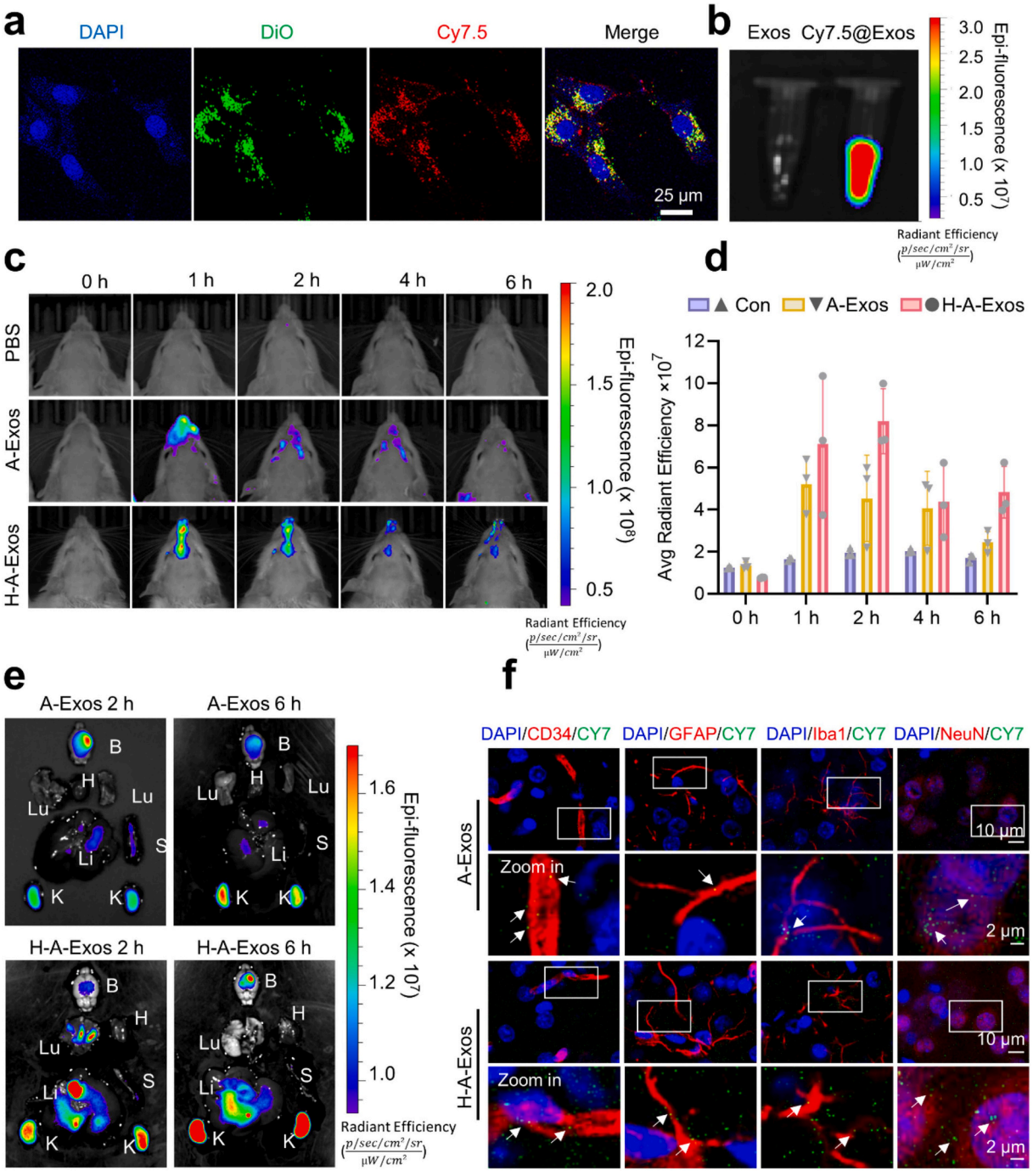


Fig. 5. The *in vivo* tracing study after intranasal administration. (a) Internalization of DiO and Cy7.5 double-labelled A-Exos. (b) The image of Cy7.5-labelled A-Exos by IVIS. (c) The tracing analysis after intranasally administration of Cy7.5-labelled A-Exos or H-A-Exos. (d) Semi-quantitative analysis of tracing fluorescence ($n = 3$). (e) Fluorescence tracing of organs (B: brain, H: heart, Li: liver, S: spleen, Lu: lungs and K: kidneys) harvested at 2 h and 6 h after intranasally administration in A-Exos and H-A-Exos group. (f) Co-localization of CY7-SE-labelled A-Exos with brain cells in the ischemic brain after intranasal administration in A-Exos and H-A-Exos group.

BBB integrity.

Further examination using TTC staining revealed red coloration in the ischemic contralateral side and white infarcts in the lateral cortex and striatum of the ischemic side (Fig. 6c). The MCAO/R group exhibited a large infarct area. Quantitative analysis showed that the infarct volume in the MCAO/R group reached 33.62 ± 1.74% (Fig. 6d). Notably, treatment with H-A-Exos further decreased the infarct volume to 13.02 ± 1.01% ($p < 0.0001$), showing superior efficacy compared with free A-Exos (17.46 ± 1.86% ($p < 0.0001$)). In contrast, NMDP reduced the infarct volume to only 25.15 ± 1.84% ($p < 0.01$). These results suggest that hydrogel-mediated sustained delivery of A-Exos markedly alleviates cerebral ischemia/reperfusion injury. NMDP, a calcium channel blocker, exerts its primary effects through vasodilation and neuroprotection. In contrast, A-Exos functions as a multi-targeted biotherapy, simultaneously promoting angiogenesis, reducing inflammation, and inhibiting apoptosis. Importantly, these results also verify that A-Exos can exert effective reparative functions in a non-tumor ischemic microenvironment, rather than being limited to tumor-associated angiogenesis. By leveraging endogenous cell-to-cell communication, A-Exos may coordinate multiple repair processes required for

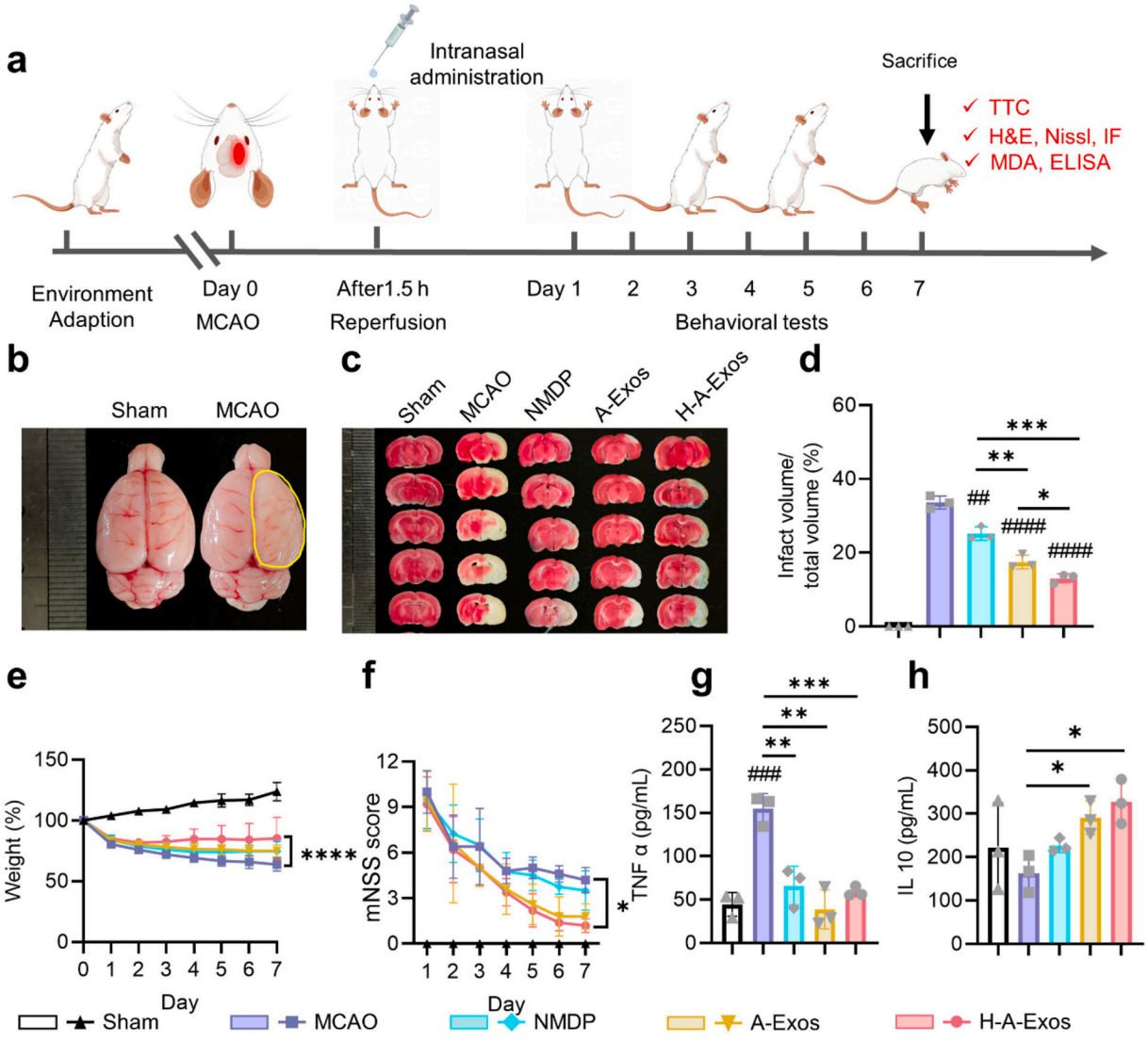


Fig. 6. Functional improvement and infarct volume reduction after treatment. (a) Illustration of experimental timeline. (b) Anatomical images of the whole brain after MCAO. The yellow circle is the infarcted ischemic area. (c) TTC-stained coronal sections after treatment and (d) quantification of infarct volume/total volume ($n = 3$). (e) mNSS scores ($n = 5$). (f) The body weight profile of rats during treatment (n = 5). (g) The extent of inflammatory factors TNF α and (h) IL10 in brain tissue as measured by ELISA (n = 3). Data are expressed as the mean ± SD, # means the contrasts between experimental groups and sham. $^{\#\#\#\#/****}p < 0.0001$, $^{\#\#\#/***}p < 0.001$, $^{\#\#/**}p < 0.01$, $^{\#/*}p < 0.05$, ns: $p > 0.05$.

neurovascular unit restoration, thereby offering inherent advantages over single-target agents such as NMDP.

Neurological recovery was assessed using the mNSS. On day 7 after MCAO/R, rats in the MCAO group still showed marked motor and sensory deficits (Fig. 6e), whereas A-Exos significantly improved neurological function and outperformed NMDP. Notably, H-A-Exos produced the lowest mNSS score (1.2 ± 0.4), indicating that hydrogel-mediated sustained delivery further enhanced A-Exos-induced neurofunctional recovery. Body weight was also monitored as an indicator of systemic recovery (Fig. 6f). Rats treated with H-A-Exos gained weight faster postoperatively than those treated with free A-Exos, while A-Exos performed better than NMDP. These results further support the superior therapeutic benefit of H-A-Exos in MCAO/R recovery.

Furthermore, inflammatory response following ischemia-reperfusion injury further complicates stroke pathology. The level of inflammatory factors in the brain tissue of each treatment group was quantified using an ELISA. Compared with the MCAO/R group, NMDP, A-Exos, and H-A-Exos significantly reduced pro-inflammatory cytokine levels (Fig. 6g). Meanwhile, A-Exos and H-A-Exos increased the expression of anti-inflammatory factors, suggesting a shift toward a reparative immune microenvironment (Fig. 6h). Compared with NMDP, which mainly acts as a calcium channel blocker to indirectly reduce vascular permeability and inflammatory infiltration, A-Exos may exert broader immunomodulatory effects through their bioactive cargo, regulating immune cell activation, intercellular communication, and the local pathological microenvironment. This multi-target regulation enables A-Exos, especially H-A-Exos, to suppress inflammatory injury more effectively, favoring their further development for clinical application.

3.7. Effects of H-A-Exos on histopathology morphology and neurological functional recovery post-MCAO

Pathological changes that occur after ischemic stroke, such as neuronal loss, apoptosis and disorganization, will lead to long-term functional deficits. These cellular changes are primarily driven by oxidative stress and inflammation. As such, attenuating these histopathological changes is essential to improve stroke recovery and brain tissue integrity. Histopathology analysis of the striatum on the ischemic side was conducted by H&E staining on day 7 after treatment. H&E staining showed that the MCAO group exhibited typical ischemic injury,

including loose and disordered tissue structure, sponge-like vacuolation, nuclear condensation, chromatin aggregation, and marked neuronal loss (Fig. 7a). In contrast, NMDP, A-Exos, and H-A-Exos treatments reduced vacuolation, improved tissue density, and restored structural organization to varying degrees. Notably, H-A-Exos showed the most pronounced improvement in tissue integrity, suggesting enhanced post-ischemic tissue repair. Nissl staining further confirmed neuronal protection (Fig. 7b). The MCAO group showed a marked reduction in Nissl bodies and severe Nissl dissolution, indicating impaired neuronal metabolism and viability. After treatment, neuronal atrophy was alleviated and Nissl body preservation improved. In particular, A-Exos and H-A-Exos retained more surviving neurons in the striatum than MCAO/R and NMDP groups, indicating stronger protection in the ischemic core region.

Additionally, Numerous TUNEL-positive cells were observed in the cortex and striatum of the MCAO group, whereas fluorescence intensity was markedly reduced after NMDP, A-Exos, and H-A-Exos treatment (Fig. 7c). Semi-quantitative analysis showed that apoptotic signals in the striatum decreased by 60.75 ± 3.25% ($p < 0.0001$) in the NMDP group, 73.53 ± 6.35% ($p < 0.0001$) in the A-Exos group, and 73.81 ± 3.79% ($p < 0.0001$) in the H-A-Exos group compared with the MCAO group (Fig. S14). As a further assessment of the safety of A-Exos and H-A-Exos, the kidneys, spleen, liver, and lungs of rats from each group were collected for histological analysis. As shown in Fig. S15, although A-Exos are derived from glioblastoma cells, no tumorigenic lesions or pathological abnormalities were observed in the brain or major organs during the experimental period, indicating good systemic biocompatibility and biosafety after intranasal administration. Nevertheless, the long-term biosafety of A-Exos remains a significant issue that has been fully acknowledged. Future research will include potential tumorigenic risks, immune responses, and organ toxicity to further evaluate its translational potential prior to clinical application.

3.8. H-A-Exos improves cerebral ischemia by promoting NVU remodeling

Functional recovery after ischemic stroke depends not on the repair of a single cell type, but on the coordinated remodeling of the neurovascular unit (NVU), which consists of neurons, glial cells, and cerebral microvessels. Therefore, the immunostaining of brain coronal sections was conducted to evaluate neuronal repair, microglial activation, and vascular regeneration following H-A-Exos treatment. NeuN immunofluorescence staining showed that H-A-Exos markedly increased the number of surviving neurons in ischemia-related brain regions, including the striatum and nucleus accumbens, compared with the MCAO/R group (Fig. 8a). Similar improvement was observed in the A-Exos group. Quantitative analysis showed that NeuN fluorescence intensity in the H-A-Exos group was 5.6-fold higher than that in the MCAO/R group, 4.3-fold higher than that in the A-Exos group, and 3.0-fold higher than that in the NMDP group (Fig. 8b), indicating that hydrogel-mediated sustained delivery further enhanced the neuroprotective effect of A-Exos. Persistent microglial activation is a major contributor to chronic inflammation and secondary neuronal injury

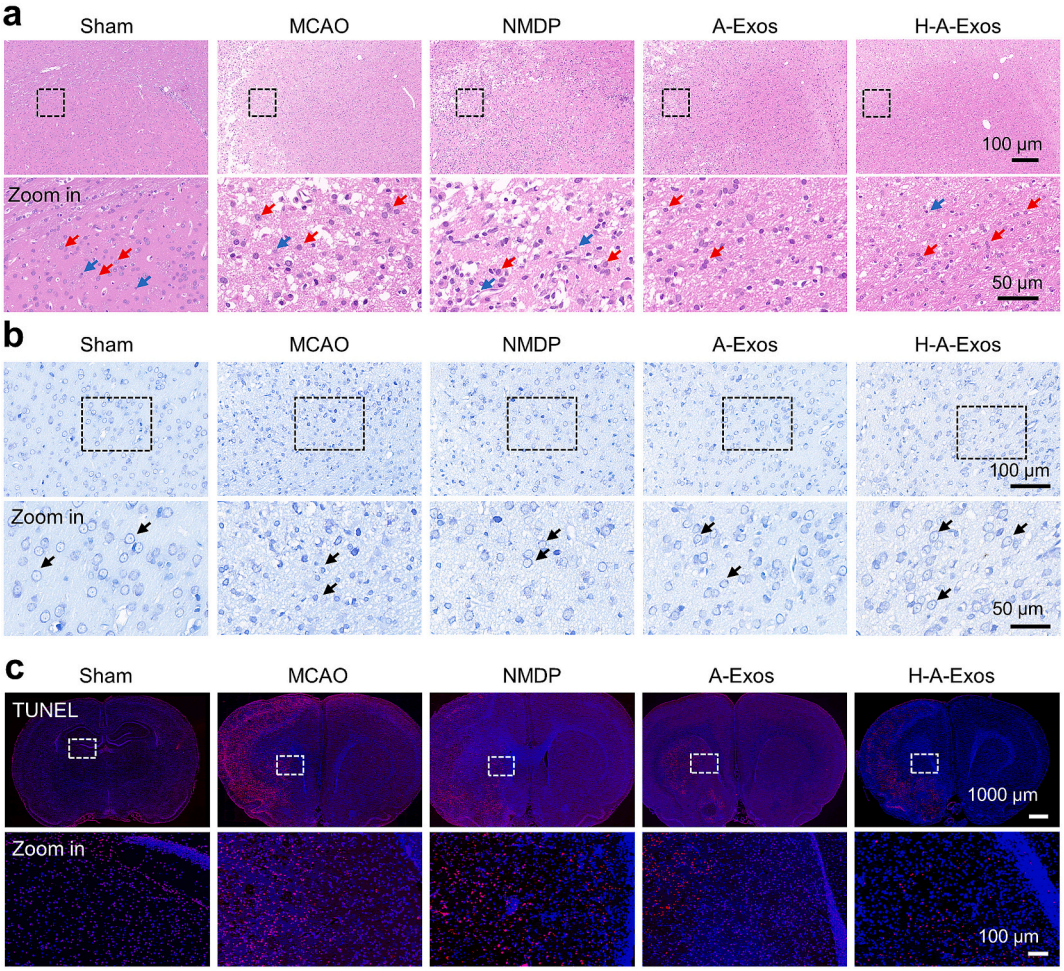


Fig. 7. Histopathological analysis after treatment of cerebral ischemia. (a) H&E staining representative images of the ischemic lateral striatum after treatment on Day 7. Red arrow: neuron cell. Blue arrow: neuroglial cell. (b) Nissl staining was analyzed in the ischemic lateral striatum. Black arrow: neuron cell. (c) TUNEL staining analysis in the ischemic lateral striatum.

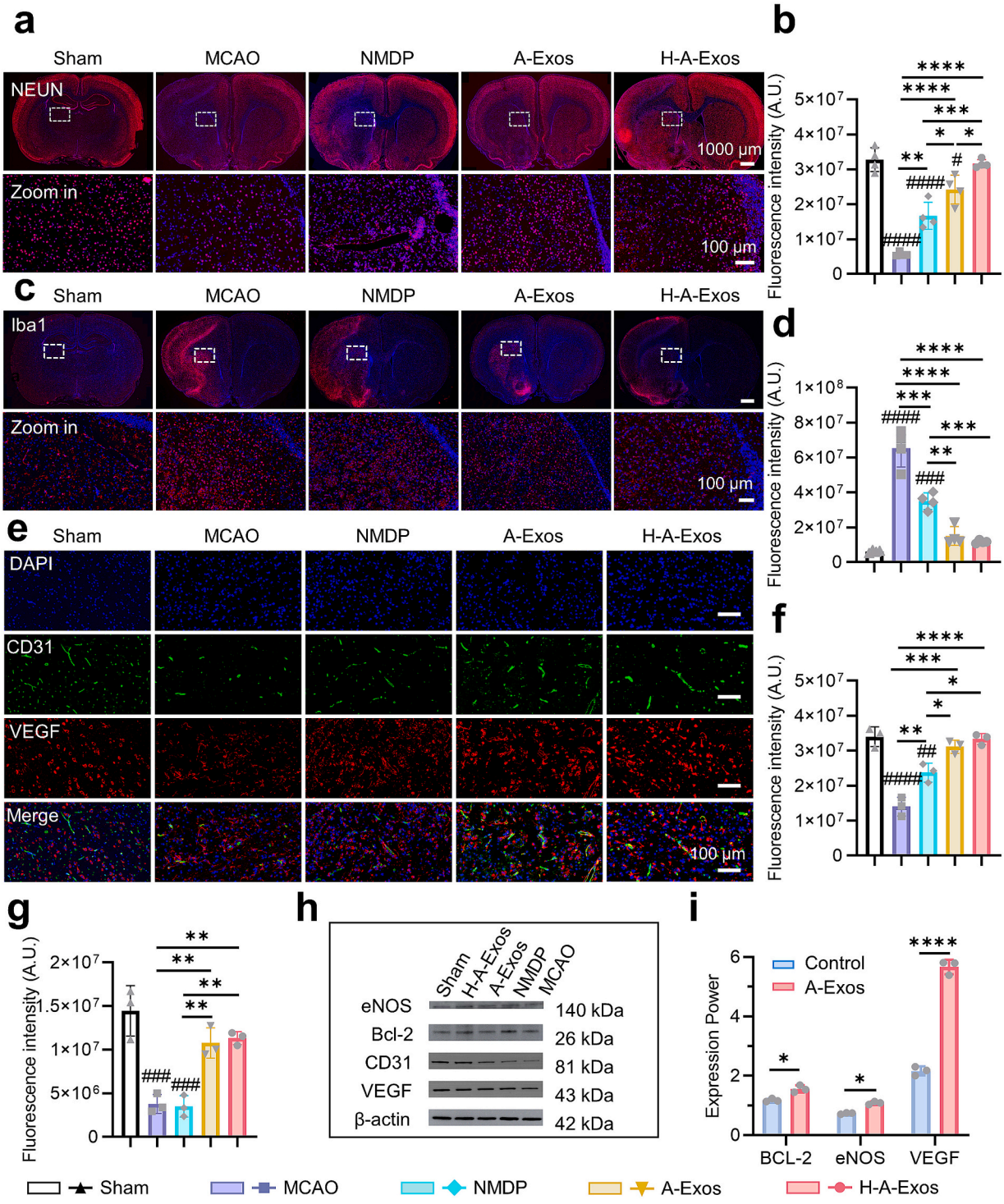


Fig. 8. H-A-Exos promotes NVU remodeling in ischemic infarct regions. (a) Representative immunostaining images of NeuN (mature neuronal cell marker, red positive cells; DAPI, nucleic marker, blue) in the ischemic lateral striatum. (b) Relative quantitative analysis of NeuN fluorescence intensity ($n = 4$). (c) Representative immunostaining images of Iba1 (microglia marker, red positive cells; DAPI, nucleic marker, blue). (d) Relative quantitative analysis of Iba1 fluorescence intensity (n = 4). (e) Immunostaining of CD31(vascular endothelial cell marker green)/VEGF (vascular endothelial growth factor, red) positive cells after treatment on Day 7. (f) Relative quantitative analysis of VEGF ($n = 3$) and (g) CD31 fluorescence intensity (n = 3). (h) WB results (eNOS, Bcl-2, CD31, VEGF) in the brain tissues after treatment. (i) Expression of mRNA detected by qPCR in HUVEC cells after treatment. Data are expressed as the mean ± SD, # means the contrasts between experimental groups and control. $^{\#\#\#\#/****}p < 0.0001$, $^{\#\#\#/***}p < 0.001$, $^{\#\#/**}p < 0.01$, $^{\#/*}p < 0.05$, ns: $p > 0.05$.

after ischemia. Iba1 immunostaining revealed extensive microglial activation in the MCAO/R group, whereas NMDP, A-Exos, and H-A-Exos treatments reduced Iba1 fluorescence intensity (Fig. 8c). Compared with the MCAO/R group, Iba1 fluorescence decreased by 81.76 ± 2.75% in the H-A-Exos group and 77.19 ± 4.82% in the A-Exos group, both approaching the sham level, while NMDP reduced it by 45.59 ± 8.53% (Fig. 8d). These results suggest that A-Exos effectively suppress excessive post-ischemic immune activation and promote inflammatory resolution, consistent with the ELISA results (Fig. 6 g, h).

Angiogenesis is another key event in NVU remodeling, supporting

oxygen and nutrient supply, neural precursor migration, and neural network reconstruction. VEGF/CD31 dual immunostaining showed that A-Exos significantly increased VEGF/CD31 double-positive cells in the ischemic region, while H-A-Exos further enhanced fluorescence intensity and positive cell numbers (Fig. 8e-g). These results indicate that A-Exos promote angiogenesis in ischemic tissue, and hydrogel-mediated sustained delivery prolongs this pro-angiogenic effect. Western blot analysis further confirmed these findings. Compared with the MCAO/R group, H-A-Exos and A-Exos treatment significantly upregulated the expression of the anti-apoptotic protein Bcl-2, endothelial function-related protein eNOS, and angiogenesis-related markers VEGF and CD31 (Fig. 8h, Fig. S16). Bcl-2 is a classical anti-apoptotic regulator, and its upregulation suggests that A-Exos effectively attenuated ischemia-induced cell apoptosis. The increased expression of eNOS indicates improved endothelial function and enhanced nitric oxide-generating capacity, which may contribute to better local perfusion in the ischemic tissue. Meanwhile, the concurrent upregulation of VEGF and CD31 further supports the pro-angiogenic effect of A-Exos, which is consistent with the immunofluorescence staining results.

In vitro validation experiment was further performed using HUVECs. Cells were serum-starved for 12 h to synchronize their status and then treated with A-Exos for 6 h, followed by qPCR analysis. As shown in Fig. 8i, A-Exos treatment significantly upregulated VEGF transcription compared with the control group. Notably, the expression levels of Bcl2 and eNOS were also elevated simultaneously. These changes are in good agreement with the protein expression patterns observed *in vivo*, further confirming that A-Exos can directly regulate angiogenesis-related gene expression in endothelial cells. Previous studies have shown that Bcl-2, eNOS, CD31 and VEGF are important downstream effectors of several classical signaling pathways involved in cell survival, angiogenesis, and tissue repair, including the PI3K/Akt, MAPK/ERK, and STAT3 pathways [66]. Therefore, the biological effects mediated by A-Exos may be associated with activation of one or more of these signaling cascades. Although the precise upstream mechanisms remain to be elucidated, the coordinated upregulation of CD31, VEGF, eNOS, and Bcl-2 suggests that A-Exos not only enhance angiogenic signaling but also protect endothelial and neurovascular cells from ischemia-induced apoptotic injury.

Collectively, these results demonstrate that A-Exos promote NVU remodeling through multi-target regulation, including neuronal preservation, inhibition of microglial overactivation, endothelial protection, and angiogenesis enhancement. The upregulation of Bcl-2, eNOS, VEGF, and CD31 suggests that A-Exos may activate pro-survival and pro-angiogenic signaling pathways, thereby restoring vascular integrity, improving local perfusion, and supporting long-term neurological recovery. Hydrogel-mediated (H-A-Exos) sustained delivery further amplifies these therapeutic effects, making H-A-Exos a promising strategy for ischemic stroke repair.

4. Conclusion

In summary, this study demonstrates the therapeutic potential of intranasally delivered H-A-Exos for cerebral ischemic injury. By integrating the pro-angiogenic bioactivity of A-Exos with the retention and sustained-release advantages of chitosan hydrogel, H-A-Exos effectively enhanced exosomes accumulation in ischemic brain regions and improved therapeutic efficacy in the MCAO/R rat model. Importantly, this study confirmed that A-Exos could exert reparative effects in a non-tumor ischemic microenvironment. Compared with free A-Exos and NMDP, H-A-Exos showed superior effects in reducing infarct volume, maintaining blood-brain barrier integrity, promoting NVU remodeling, and improving neurological and systemic recovery. Mechanistically, H-A-Exos upregulated key molecules associated with vascular regeneration and cell survival, including VEGF, CD31, eNOS, and Bcl-2, thereby contributing to vascular reconstruction, neurostructural repair, and restoration of post-ischemic homeostasis. These findings suggest that H-A-Exos functions as a multi-target biological therapy capable of coordinating the complex repair processes required for ischemic stroke recovery. Overall, intranasal delivery of H-A-Exos provides a non-invasive and brain-targeted strategy for NVU restoration and ischemia/reperfusion injury management. Future studies should further identify the key active components within A-Exos, such as specific miRNAs or proteins, optimize dosing regimens, and evaluate long-term biosafety to support clinical translation.

CRediT authorship contribution statement

Lifei Huang: Writing – original draft, Visualization, Methodology, Investigation, Data curation. **Zhihan Liu:** Validation, Investigation. **Quanrui Zhang:** Validation, Investigation. **Wensheng Xie:** Formal analysis. **Guofeng Li:** Methodology, Formal analysis. **Junhao Yan:** Writing – review & editing, Formal analysis. **Meng Qin:** Writing – review & editing, Supervision, Funding acquisition, Formal analysis. **Xing Wang:** Writing – review & editing, Supervision, Funding acquisition, Conceptualization.

Declaration of competing interest

The authors declare that they have no known competing financial interests or personal relationships that could have appeared to influence the work reported in this paper.

Acknowledgements

This work was supported by Key Program of Beijing Natural Science Foundation (grant number Z200025), National Natural Science Foundation of China (NSFC52473137).

Appendix A. Supplementary data

Supplementary data to this article can be found online at https://doi.org/10.1016/j.ijbiomac.2026.153517.

Data availability

Data will be made available on request.

References

[1] B.C.V. Campbell, D.A. De Silva, M.R. Macleod, et al., Ischaemic stroke, Nat. Rev. Dis. Prim. 5 (1) (2019) 70, https://doi.org/10.1038/s41572-019-0118-8.
[2] B.R.S. Broughton, D.C. Reutens, C.G. Sobey, Apoptotic mechanisms after cerebral ischemia, Stroke 40 (2009) e331–e339, https://doi.org/10.1161/STROKEAHA.108.531632.
[3] V.L. Feigin, B. Norrving, G.A. Mensah, Global burden of stroke, Circ. Res. 120 (3) (2017) 439–448, https://doi.org/10.1161/CIRCRESAHA.116.308413.
[4] Q. Zhang, M. Jia, Y. Wang, et al., Cell death mechanisms in cerebral ischemia–reperfusion injury, Neurochem. Res. 47 (12) (2022) 3525–3542, https://doi.org/10.1007/s11064-022-03697-8.
[5] D.O. Kleindorfer, A. Towfighi, S. Chaturvedi, et al., 2021 guideline for the prevention of stroke in patients with stroke and transient ischemic attack: a guideline from the american heart association/american stroke association, Stroke 52 (2021) e364–e467, https://doi.org/10.1161/STR.0000000000000375.
[6] V. Saini, L. Guada, D.R. Yavagal, Global epidemiology of stroke and access to acute ischemic stroke interventions, Neurology 97 (20_Supplement_2) (2021) S6–S16, https://doi.org/10.1212/WNL.0000000000012781.
[7] C.P. Sperring, W.M. Savage, M.G. Argenziano, et al., No-reflow post-recanalization in acute ischemic stroke: mechanisms, measurements, and molecular markers, Stroke 54 (9) (2023) 2472–2480, https://doi.org/10.1161/STROKEAHA.123.044240.
[8] D. Barthels, H. Das, Current advances in ischemic stroke research and therapies, Biochim. Biophys. Acta (BBA) - Mol. Basis Dis. 1866 (4) (2020) 165260, https://doi.org/10.1016/j.bbadis.2018.09.012.
[9] R.H.C. Lee, M.H.H. Lee, C.Y.C. Wu, et al., Cerebral ischemia and neuroregeneration, Neural Regen. Res. 13 (3) (2018) 373, https://doi.org/10.4103/1673-5374.228711.
[10] C. Chugh, Acute ischemic stroke: management approach, Indian Journal of Critical Care 23 (Suppl. 2) (2019) S140–S146, https://doi.org/10.5005/jp-journals-10071-23192.

[11] P. Jolugbo, R.A.S. Ariëns, Thrombus composition and efficacy of thrombolysis and thrombectomy in acute ischemic stroke, Stroke 52 (3) (2021) 1131–1142, https://doi.org/10.1161/STROKEAHA.120.032810.
[12] Peña I. Dela, C. Borlongan, G. Shen, et al., Strategies to extend thrombolytic time window for ischemic stroke treatment: an unmet clinical need, Journal of Stroke 19 (1) (2017) 50–60, https://doi.org/10.5853/jos.2016.01515.
[13] P.D. Lyden, Thrombolytic therapy for acute ischemic stroke: a very great honor, Stroke 50 (9) (2019) 2597–2603, https://doi.org/10.1161/STROKEAHA.119.025699.
[14] L. La, X. Wa, Z. Ya, Ischemia-reperfusion injury in the brain: mechanisms and potential therapeutic strategies, Biochem. Pharmacol. 5 (4) (2016) 213, https://doi.org/10.4172/2167-0501.1000213.
[15] T. Kalogeris, C.P. Baines, M. Krenz, et al., Ischemia/reperfusion, Compr. Physiol. 7 (1) (2016) 113–170, https://doi.org/10.1002/cphy.c160006.
[16] S. Schaeffer, C. Iadecola, Revisiting the neurovascular unit, Nat. Neurosci. 24 (9) (2021) 1198–1209, https://doi.org/10.1038/s41593-021-00904-7.
[17] X. Yu, C. Ji, A. Shao, Neurovascular unit dysfunction and neurodegenerative disorders, Front. Neurosci. 14 (2020) 334, https://doi.org/10.3389/fnins.2020.00334.
[18] N.J. Alkayed, M.J. Cipolla, The ever-evolving concept of the neurovascular unit, Stroke 54 (8) (2023) 2178–2180, https://doi.org/10.1161/STROKEAHA.123.042705.
[19] L. Wang, X. Xiong, L. Zhang, et al., Neurovascular unit: a critical role in ischemic stroke, CNS Neurosci. Ther. 27 (1) (2021) 7–16, https://doi.org/10.1111/cns.13561.
[20] S. Tiedt, A.M. Buchan, M. Dichgans, et al., The neurovascular unit and systemic biology in stroke—implications for translation and treatment, Nat. Rev. Neurol. 18 (10) (2022) 597–612, https://doi.org/10.1038/s41582-022-00703-z.
[21] B.C. Smith, R.A. Tinkey, B.C. Shaw, et al., Targetability of the neurovascular unit in inflammatory diseases of the central nervous system, Immunol. Rev. 311 (1) (2022) 39–49, https://doi.org/10.1111/imr.13121.
[22] Z.G. Zhang, B. Buller, M. Chopp, Exosomes — beyond stem cells for restorative therapy in stroke and neurological injury, Nat. Rev. Neurol. 15 (4) (2019) 193–203, https://doi.org/10.1038/s41582-018-0126-4.
[23] J. Fang, Z. Wang, C. Miao, Angiogenesis after ischemic stroke, Acta Pharmacol. Sin. 44 (7) (2023) 1305–1321, https://doi.org/10.1038/s41401-023-01061-2.
[24] A. Ergul, A. Alhusban, S.C. Fagan, Angiogenesis, Stroke 43 (8) (2012) 2270–2274, https://doi.org/10.1161/STROKEAHA.111.642710.
[25] D.A. Greenberg, K. Jin, From angiogenesis to neuropathology, Nature 438 (7070) (2005) 954–959, https://doi.org/10.1038/nature04481.
[26] A.M. Zagrean, D.M. Hermann, I. Opris, et al., Multicellular crosstalk between exosomes and the neurovascular unit after cerebral ischemia. Therapeutic implications, Front. Neurosci. 12 (2018) 811, https://doi.org/10.3389/fnins.2018.00811.
[27] C. Davis, S.I. Savitz, N. Satani, Mesenchymal stem cell derived extracellular vesicles for repairing the neurovascular unit after ischemic stroke, Cells 10 (4) (2021) 767, https://doi.org/10.3390/cells10040767.
[28] J. Gregorius, C. Wang, O. Stambouli, et al., Small extracellular vesicles obtained from hypoxic mesenchymal stromal cells have unique characteristics that promote cerebral angiogenesis, brain remodeling and neurological recovery after focal cerebral ischemia in mice, Basic Res. Cardiol. 116 (1) (2021) 40, https://doi.org/10.1007/s00395-021-00881-9.
[29] Y. Zhang, Y. Qin, M. Chopp, et al., Ischemic cerebral endothelial cell-derived exosomes promote axonal growth, Stroke 51 (12) (2020) 3701–3712, https://doi.org/10.1161/STROKEAHA.120.031728.
[30] Z. Liu, Q. Xia, C. Wang, et al., Biomimetic astrocyte cell membrane-fused nanovesicles for protecting neurovascular units in hypoxic ischemic encephalopathy, J. Nanobiotechnol. 22 (1) (2024) 766, https://doi.org/10.1186/s12951-024-03053-8.
[31] J. Pan, S. Sheng, L. Ye, et al., Extracellular vesicles derived from glioblastoma promote proliferation and migration of neural progenitor cells via pi3k-akt pathway, Cell Commun. Signal 20 (1) (2022) 7, https://doi.org/10.1186/s12964-021-00760-9.
[32] N. Ludwig, S.S. Yerneni, J.H. Azambuja, et al., Tumor-derived exosomes promote angiogenesis via adenosine a2b receptor signaling, Angiogenesis 23 (4) (2020) 599–610, https://doi.org/10.1007/s10456-020-09728-8.
[33] S. Maacha, A.A. Bhat, L. Jimenez, et al., Extracellular vesicles-mediated intercellular communication: roles in the tumor microenvironment and anti-cancer drug resistance, Mol. Cancer 18 (1) (2019) 55, https://doi.org/10.1186/s12943-019-0965-7.
[34] Z.-F. Wang, F. Liao, H. Wu, et al., Glioma stem cells-derived exosomal mir-26a promotes angiogenesis of microvessel endothelial cells in glioma, J. Exp. Clin. Cancer Res. 38 (1) (2019) 201, https://doi.org/10.1186/s13046-019-1181-4.
[35] A. Monteforte, B. Lam, M.B. Sherman, et al., Glioblastoma exosomes for therapeutic angiogenesis in peripheral ischemia, Tissue Eng. A 23 (21−22) (2017) 1251–1261, https://doi.org/10.1089/ten.tea.2016.0508.
[36] Z.-J. Yang, Q.-C. Bi, L.-J. Gan, et al., Exosomes derived from glioma cells under hypoxia promote angiogenesis through up-regulated exosomal connexin 43, Int. J. Med. Sci. 19 (7) (2022) 1205–1215, https://doi.org/10.7150/ijms.71912.
[37] R. Lucero, V. Zappulli, A. Sammarco, et al., Glioma-derived miRNA-containing extracellular vesicles induce angiogenesis by reprogramming brain endothelial cells, Cell Rep. 30 (7) (2020) 2065–2074.e4, https://doi.org/10.1016/j.celrep.2020.01.073.
[38] Z. Xue, J. Liu, W. Xing, et al., Hypoxic glioma-derived exosomal mir-25-3p promotes macrophage m2 polarization by activating the pi3k-akt-mtor signaling pathway, J. Nanobiotechnol. 22 (1) (2024) 628, https://doi.org/10.1186/s12951-024-02888-5.
[39] J. Xu, J. Zhang, Z. Zhang, et al., Hypoxic glioma-derived exosomes promote m2-like macrophage polarization by enhancing autophagy induction, Cell Death Dis. 12 (4) (2021) 1–16, https://doi.org/10.1038/s41419-021-03664-1.
[40] M. Qian, S. Wang, X. Guo, et al., Hypoxic glioma-derived exosomes deliver microrna-1246 to induce m2 macrophage polarization by targeting terf2ip via the stat3 and nf-κb pathways, Oncogene 39 (2) (2020) 428–442, https://doi.org/10.1038/s41388-019-0996-y.
[41] S. Ray, M. Kumar, D.T. Chemparathy, et al., HIF-1 targeting intervention renders protection from Alzheimer's-like pathology in a humanized mice model of HIV infection, J. Extracell. Vesicles 14 (11) (2025) e70191.
[42] Y. Chen, C. Zhang, Y. Huang, et al., Intranasal drug delivery: the interaction between nanoparticles and the nose-to-brain pathway, Adv. Drug Deliv. Rev. 207 (2024) 115196, https://doi.org/10.1016/j.addr.2024.115196.
[43] N. Rabiee, S. Ahmadi, R. Afshari, et al., Polymeric nanoparticles for nasal drug delivery to the brain: relevance to Alzheimer's disease, Advanced Therapeutics 4 (3) (2021) 2000076, https://doi.org/10.1002/adtp.202000076.
[44] E. Nance, S.H. Pun, R. Saigal, et al., Drug delivery to the central nervous system, Nature Reviews Materials 7 (4) (2022) 314–331, https://doi.org/10.1038/s41578-021-00394-w.
[45] D. Furtado, M. Björnmalm, S. Ayton, et al., Overcoming the blood–brain barrier: the role of nanomaterials in treating neurological diseases, Adv. Mater. 30 (46) (2018) 1801362, https://doi.org/10.1002/adma.201801362.
[46] R. Pandit, L. Chen, J. Götz, The blood-brain barrier: physiology and strategies for drug delivery, Adv. Drug Deliv. Rev. 165–166 (2020) 1–14, https://doi.org/10.1016/j.addr.2019.11.009.
[47] D. Wu, Q. Chen, X. Chen, et al., The blood–brain barrier: structure, regulation and drug delivery, Signal Transduct. Target. Ther. 8 (1) (2023) 1–27, https://doi.org/10.1038/s41392-023-01481-w.
[48] G.C. Terstappen, A.H. Meyer, R.D. Bell, et al., Strategies for delivering therapeutics across the blood–brain barrier, Nat. Rev. Drug Discov. 20 (5) (2021) 362–383, https://doi.org/10.1038/s41573-021-00139-y.
[49] E.G. Knox, M.R. Aburto, G. Clarke, et al., The blood-brain barrier in aging and neurodegeneration, Mol. Psychiatry 27 (6) (2022) 2659–2673, https://doi.org/10.1038/s41380-022-01511-z.
[50] J.J. Lochhead, R.G. Thorne, Intranasal delivery of biologics to the central nervous system, Adv. Drug Deliv. Rev. 64 (7) (2012) 614–628, https://doi.org/10.1016/j.addr.2011.11.002.
[51] A.R. Khan, M. Liu, M.W. Khan, et al., Progress in brain targeting drug delivery system by nasal route, J. Control. Release 268 (2017) 364–389, https://doi.org/10.1016/j.jconrel.2017.09.001.
[52] S. Mignani, X. Shi, A. Karpus, et al., Non-invasive intranasal administration route directly to the brain using dendrimer nanoplatforms: an opportunity to develop new CNS drugs, Eur. J. Med. Chem. 209 (2021) 112905, https://doi.org/10.1016/j.ejmech.2020.112905.
[53] Y. Li, H. Wu, X. Jiang, et al., New idea to promote the clinical applications of stem cells or their extracellular vesicles in central nervous system disorders: combining with intranasal delivery, Acta Pharm. Sin. B 12 (8) (2022) 3215–3232, https://doi.org/10.1016/j.apsb.2022.04.001.
[54] J. Li, H. Zhang, Y. Jiang, et al., The landscape of extracellular vesicles combined with intranasal delivery towards brain diseases, Nano Today 55 (2024) 102169, https://doi.org/10.1016/j.nantod.2024.102169.
[55] T. Ikeda, M. Kawabori, Y. Zheng, et al., Intranasal administration of mesenchymal stem cell-derived exosome alleviates hypoxic-ischemic brain injury, Pharmaceutics 16 (4) (2024) 446, https://doi.org/10.3390/pharmaceutics16040446.
[56] Y. Wang, H. Niu, L. Li, et al., Anti-chac1 exosomes for nose-to-brain delivery of mir-760-3p in cerebral ischemia/reperfusion injury mice inhibiting neuron ferroptosis, J. Nanobiotechnol. 21 (1) (2023) 109, https://doi.org/10.1186/s12951-023-01862-x.
[57] X. Zhou, X. Deng, M. Liu, et al., Intranasal delivery of BDNF-loaded small extracellular vesicles for cerebral ischemia therapy, J. Control. Release 357 (2023) 1–19, https://doi.org/10.1016/j.jconrel.2023.03.033.
[58] Y. Fu, Y. Li, B. Deng, et al., Spatiotemporally dynamic therapy with shape-adaptive drug-gel for the improvement of tissue regeneration with ordered structure, Bioact. Mater. 8 (2022) 165–176.
[59] Paul M. Holloway, F.N. Gavins, Modeling ischemic stroke in vitro: status quo and future perspectives, Stroke 47 (2) (2016) 561–569, https://doi.org/10.1161/STROKEAHA.115.011932.
[60] Q. Mu, K. Yao, M.Z. Syeda, et al., Ligustrazine nanoparticle hitchhiking on neutrophils for enhanced therapy of cerebral ischemia-reperfusion injury, Adv. Sci. 10 (19) (2023) 2301348, https://doi.org/10.1002/advs.20230134.
[61] Y. Zhang, M. Jiang, M. Wei, et al., $MgSO_4$ as a novel hypothermia infusion solution promotes ischemic stroke recovery through Ca^{2+} regulation of neurovascular units, Theranostics 15 (5) (2025) 1896, https://doi.org/10.7150/THNO.104879.
[62] X. Ni, H. Wang, Y. Cai, et al., Ginsenoside Rb1 inhibits astrocyte activation and promotes transfer of astrocytic mitochondria to neurons against ischemic stroke, Redox Biol. 54 (2022) 102363, https://doi.org/10.1016/j.redox.2022.102363.
[63] K. Urbańska, A. Orzechowski, Unappreciated role of LDHA and LDHB to control apoptosis and autophagy in tumor cells, Int. J. Mol. Sci. 20 (9) (2019) 2085, https://doi.org/10.3390/ijms20092085.

[64] Z. Liu, Z. Wang, Z. Zhu, et al., Crocetin regulates functions of neural stem cells to generate new neurons for cerebral ischemia recovery, Adv. Healthc. Mater. 12 (20) (2023) 2203132, https://doi.org/10.1002/adhm.202203132.
[65] L.V. Vossen, M. Weiss, W. Albanna, et al., Intra-arterial nimodipine for the treatment of refractory delayed cerebral ischemia after aneurysmal subarachnoid hemorrhage, Journal of NeuroInterventional Surgery 17 (e1) (2025) e31–e40, https://doi.org/10.1136/jnis-2023-021151.
[66] K. Moeinabadi-Bidgoli, M. Rezaee, N. Hossein-Khannazer, et al., Exosomes for angiogenesis induction in ischemic disorders, J. Cell. Mol. Med. 27 (6) (2023) 763–787.